BIOCHEMISTRY
including biophysical chemistry & molecular biology

Article

pubs.acs.org/biochemistry

Constraints on the Radical Cation Center of Cytochrome *c* Peroxidase for Electron Transfer from Cytochrome *c*

Thomas M. Payne,[†] Estella F. Yee,[†] Boris Dzikovski,[†,‡] and Brian R. Crane*[,†]

[†]Department of Chemistry and Chemical Biology, Cornell University, Ithaca, New York 14853, United States

[‡]National Biomedical Center for Advanced ESR Technologies (ACERT), Cornell University, Ithaca, New York 14850, United States

ABSTRACT: The tryptophan 191 cation radical of cytochrome *c* peroxidase (CcP) compound I (Cpd I) mediates long-range electron transfer (ET) to cytochrome *c* (Cc). Here we test the effects of chemical substitution at position 191. CcP W191Y forms a stable tyrosyl radical upon reaction with peroxide and produces spectral properties similar to those of Cpd I but has low reactivity toward reduced Cc. CcP W191G and W191F variants also have low activity, as do redox ligands that bind within the W191G cavity. Crystal structures of complexes between Cc and CcP W191X (X = Y, F, or G), as well as W191G with four bound ligands reveal similar 1:1 association modes and heme pocket conformations. The ligands display structural disorder in the pocket and do not hydrogen bond to Asp235, as does Trp191. Well-ordered Tyr191 directs its hydroxyl group toward the porphyrin ring, with no basic residue in the range of interaction. CcP W191X (X = Y, F, or G) variants substituted with zinc-porphyrin (ZnP) undergo photoinduced ET with Cc(III). Their slow charge recombination kinetics that result from loss of the radical center allow resolution of difference spectra for the charge-separated state [ZnP^+, Cc(II)]. The change from a phenyl moiety at position 191 in W191F to a water-filled cavity in W191G produces effects on ET rates much weaker than the effects of the change from Trp to Phe. Low net reactivity of W191Y toward Cc(II) derives either from the inability of ZnP^+ or the Fe-CcP ferryl to oxidize Tyr or from the low potential of the resulting neutral Tyr radical.

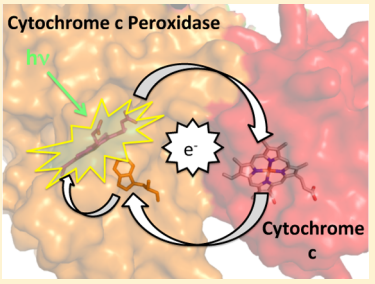

The electron transfer (ET) partners cytochrome *c* peroxidase (CcP) and cytochrome *c* (Cc) provide an important model system for understanding interprotein ET, protein−protein interactions, and heme−oxygen chemistry.[1−6] The catalytic mechanism of CcP:Cc proceeds as follows: Peroxide reacts with the Fe(III) heme of CcP to form compound I (Cpd I), which consists of an Fe(IV) iron oxo species [Fe(IV)═O] and a radical cation localized on neighboring Trp191 ($W^{\bullet+}$). Two Fe(II) Cc proteins sequentially reduce CcP Cpd I back to Fe(III) and water. In the first step, $W^{\bullet+}$ is directly reduced by Cc(II). In the second step, the remaining Fe(IV)═O center reoxidizes Trp191, which is subsequently reduced by Cc(II)[7−10] (Scheme 1). Thus, $W^{\bullet+}$ is the key electron acceptor for oxidation of Cc(II). Hoffman and colleagues developed CcP:Cc as a model ET system by incorporating Zn-porphyrin (ZnP) into either CcP or Cc in place of heme.[2,11−16] The photoexcited ZnP triplet state injects an electron across the molecular interface to reduce the Cc Fe(III) heme. ZnP^+ and Cc(II) then recombine to regenerate the ground state. Similar to the native reaction, back ET between ZnP^+ and Cc(II) is greatly accelerated by Trp191, which acts as a hole-hopping site by localizing the cation radical closer to the Cc Fe(II) heme[3,17−19] (Figure 1). Little of the charged separated state builds up in ZnCcP:Cc because the rate constant for back ET (k_{eb}) is much greater than the rate constant for forward ET (k_e). However, the W191F substitution slows ET by at least 2 orders of magnitude and allows resolution of a ZnP^+ Cc(II) intermediate.[17,20] In fact, charge recombination in W191F is slow enough to compete with complex dissociation, which produces a second kinetic phase at long times.[20] Recent theoretical studies support the involvement of Trp191 oxidation in ZnCcP:Cc reaction kinetics.[3,19] Importantly, the back reaction of the $ZnP/W^{\bullet+}$ center with Fe(II)Cc involves donor−acceptor states, redox potentials, and coupling pathways similar to those of the natural ET reaction between Cpd I and Fe(II)Cc.[3]

Conformational processes and dynamic docking of the CcP:Cc complex have also attracted much interest.[5,9,21−30] Photoinduced ET reactions in crystals confirm that the crystal association mode has ET kinetics similar those observed in solution.[18,31,32] Nonetheless, conformational dynamics within the ZnCcP:Cc complex likely generate ET competent states both in solution and in crystals.[5,18,31,33,34] Altered binding

Scheme 1. Peroxidase Activity of CcP and Cc

$$Fe(III)CcP + HOOH \rightarrow Fe(IV)=O,W^{\bullet+}CcP + H_2O \quad (1)$$

$$Fe(IV)=O,W^{\bullet+}CcP + Fe(II)Cc \rightarrow Fe(IV)=O,W^{0}CcP + Fe(III)Cc \quad (2)$$

$$Fe(IV)=O,W^{0}CcP + H^+ \rightarrow Fe(III)\text{-}OH,W^{\bullet+}CcP \quad (3)$$

$$Fe(III)\text{-}OH,W^{\bullet+}CcP + Fe(II)Cc + H^+ \rightarrow Fe(III),W^{0}CcP + Fe(III)Cc + H_2O \quad (4)$$

Received: March 22, 2016
Revised: August 6, 2016
Published: August 6, 2016

DOI: 10.1021/acs.biochem.6b00262
Biochemistry 2016, 55, 4807−4822

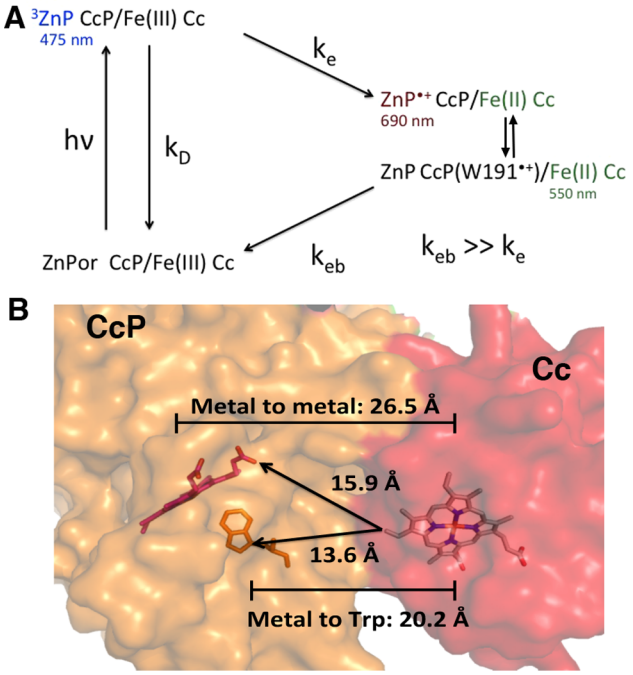

Figure 1. Photoinduced ET by ZnCcP:Cc. (A) The triplet state of zinc-porphyrin (ZnP) bound to CcP (^{3}ZnP) is produced by an 8 ns pulse of 532−560 nm light. ^{3}ZnP CcP will then either decay back to the ground state (rate constant k_D in the absence of Cc) or reduce Fe(III)Cc to Fe(II)Cc (rate constant k_e) to produce a porphyrin radical cation (ZnP$^+$). The cation radical rapidly equilibrates between ZnP$^+$ and a nearby aromatic side chain at position 191. The charge-separated state will then recombine with rate constant k_{eb}. Dissociation and reassociation of the charge-separated complex are not included in the scheme. (B) Residue 191 resides between the CcP ZnP and Cc heme in the protein complex.

interactions between CcP and Cc cause changes in ET kinetics that can be explained by accounting for Trp191 radical formation, electron coupling between donor and acceptor sites, redox potentials, and reorganization energies.[3]

Electron−hole hopping through aromatic residues is an important process in many redox systems such as photosystem II, ribonucleotide reductase (RR), photolyase enzymes, and cryptochromes.[35−41] Protein ET rate constants are exponentially dependent on the distance of separation between electron donor (D) and acceptor (A) sites.[42] Thus, if the acceptor can oxidize an intervening residue (the "hole"), one long ET step can be broken into two shorter "hops".[37,43−45] Introduction of appropriately placed Trp and Tyr residues into modified blue copper proteins[44−46] and model systems[36,47] demonstrates the ability of aromatic residues to accelerate long-range ET. Incorporation of non-natural variants of Tyr into RR has also probed the effects of redox potential on multistep tunneling reactions.[40] ZnCcP:Cc provides another system for exploring residue oxidation in ET with the potential advantage of widening the reactivity of the hole-hopping site beyond Tyr and Trp residues. In particular, Goodin and colleagues have demonstrated that the Trp191Gly variant (W191G) produces a cavity in CcP within which heterocyclic cationic compounds will bind.[48−51] One such compound, 2-aminothiazole, acts as a reductant of the peroxide-oxidized heme.[50] Replacement of a segment of the CcP polypeptide with a surrogate peptide allows for substitution of Trp191 with benzimidazole.[52] Despite being a good structural mimic for the native residues, the surrogate peptide renders CcP inactive because the benzimidazole moiety cannot form a stable radical upon reaction with peroxide.[52] Herein, we extend this general approach of CcP cavity complementation to examine the ability of residue substitutions and exogenous compounds to support peroxidase activity and hole hopping in ZnCcP:Cc. Determinations of the structures of modified CcP:Cc complexes provide constraints for the interpretation of reactivity. We find that despite wild-type (WT)-like conformations and suitable redox potentials of various exogenous surrogates, only the native Trp191 residue supports peroxidase activity with Cc and rapid back ET in the ZnCcP system. Surprisingly, a Tyr191 variant also appears to form a Cpd I-like state but does not oxidize Cc in the natural reaction or accelerate the photoinduced recombination process.

EXPERIMENTAL PROCEDURES

Mutagenesis. Cytochrome *c* peroxidase (CcP) was subcloned into the ppSUMO vector,[53] a pET28 derivative vector that introduces a His-tagged version of the SUMO protein into the N-terminus of CcP (obtained from H. Sondermann, Department of Molecular Medicine, Cornell University). After a silent mutation (QuikChange, Agilent Technologies) was introduced to remove a natural BamHI site in CcP, the CcP gene was amplified via polymerase chain reaction and inserted between the BamHI and XhoI restriction sites of ppSUMO. Two N-terminal Met-Ile residues were added to generate the "MI" version of CcP.[24] Point mutations were introduced via QuikChange (Agilent Technologies).

Protein Purification. Cytochrome *c* was expressed and purified as described previously.[54] *Escherichia coli* BL21(DE3) cells were transformed with the Cc gene in a PBTR-1 vector and expressed overnight at 37 °C in lysogeny broth (LB) with 125 μg/mL ampicillin and 50 μg/mL δ-aminolevulenic acid to increase heme production. The PBTR1 vector[54] contains the *trc* promoter, which is constitutively active and does not require induction. Cells were harvested by centrifugation at 8000 rpm, and pellets were resuspended in 50 mM sodium phosphate (pH 8.0). The resuspended pellets were either frozen for storage or lysed by sonication. The lysate was spun at 22000 rpm for 1 h to remove insoluble cell detritus, and the supernatant was loaded directly onto a HiPrep CMFF cation exchange column (GE Healthcare Life Sciences) using an ÄKTA FPLC system (Amersham Pharmacia). The column was equilibrated and washed with 50 mM sodium phosphate (pH 8), and Cc was eluted by a 5 column volume gradient of a high-salt buffer [50 mM sodium phosphate (pH 8) and 500 mM NaCl]. All red-colored fractions were collected and concentrated using Millipore Amicon Ultra centrifugal concentrators (10 kDa cutoff) and then loaded onto a Superdex 75 size-exclusion column [50 mM sodium phosphate (pH 8) and 500 mM NaCl]. Red-colored fractions were concentrated, flash-frozen, and stored at −80 °C.

Cytochrome *c* peroxidase was expressed in BL21(DE3) cells and grown at 37 °C in LB with 50 μg/mL kanamycin. When the OD_{600} reached 0.8−1.2, cells were induced with 100 μM isopropyl β-D-1-thiogalactopyranoside and overexpressed at 24 °C for ∼20 h. Cells were harvested by centrifugation at 8000 rpm, and the pellets were resuspended in lysis buffer [50 mM HEPES (pH 7.0), 150 mM NaCl, and 5 mM imidazole]. Cells were lysed by sonication. Insoluble cell detritus was separated out by centrifugation at 22000 rpm for 1 h. CcP was purified with a Ni-NTA column (Qiagen). To cleave the SUMO tag, the ULP-1 protease was added to the elution and incubated at 4

DOI: 10.1021/acs.biochem.6b00262
Biochemistry 2016, 55, 4807−4822

°C overnight. The eluent was then dialyzed into 100 mM potassium phosphate (KP_i, pH 6) buffer and passed over the Ni-NTA resin to separate the cleaved tag from the protein. CcP was loaded onto a HiPrep Q anion exchange column (GE Healthcare Life Sciences) using an AKTA FPLC system. A 10 column volume gradient of 100 mM KP_i against 500 mM KP_i (pH 6.0) was used to separate the heme-containing CcP (FeCcP) from the apo-CcP. The apo-CcP was collected for zinc-protoporphyrin IX (ZnP) incorporation. FeCcP was concentrated and stored at −80 °C for enzymatic assays. To improve the yield of heme incorporation, SUMO-cleaved CcP in 100 mM KP_i (pH 6) was gently stirred with 1 molar equivalent of hemin (stock dissolved in 0.1 M NaOH) at 4 °C overnight. The reaction mixture was neutralized with 1 molar equivalent of 0.1 M acetic acid afterward and centrifuged to remove the precipitate. The solution was run through an equilibrated Superdex 75 SEC column followed by anion exchange chromatography to separate the iron-containing protein from the apoprotein.[55]

For ZnP incorporation, the apo-CcP concentration was determined using the absorbance at 280 nm and a molar absorptivity coefficient ε_{280} of 55 mM^{-1} cm^{-1}.[56] A 5-fold excess of ZnP and carbonyl-diimidazole (1:1 molar ratio) was mixed with apo-CcP in THF or DMF for 2 h. The solvent was removed by rotovap and the activated ZnP resuspended in 500 μL of DMF. The ZnP solution was added to the apo-CcP and allowed to stir in the dark for 5 days at 4 °C. The solution was then centrifuged to remove protein and unbound ZnP that had precipitated. The sample was loaded onto the Superdex 75 size-exclusion column in 100 mM KP_i (pH 6.0) to increase purity and to remove nonspecifically bound ZnP. The colored fractions were concentrated and loaded onto the HiPrep Q column to separate the apoprotein from the ZnP-incorporated protein (ZnCcP) using the protocol described previously to separate the apo-CcP from FeCcP. ZnP incorporation was evaluated by comparing the UV−vis absorbance of the protein peak at 280 nm and the ZnCcP Soret peak at 432 nm (ε_{432} = 196 mM^{-1} cm^{-1}).[13,57] Fractions with an A_{432}/A_{280} ratio of >2 were concentrated, flash-frozen, and stored at −80 °C for crystallization and spectroscopy. Yields of ZnCcP were 80−90% of the initial apoprotein.

Crystallography. Prior to crystallization, Fe(III)CcP and Cc were combined in a 1:1 molar ratio at a final concentration of 1 mM each. The protein mixture was buffer exchanged into H_2O to reduce the ionic strength and thereby increase the level of CcP/Cc binding. Initial crystal hits were obtained using the Phoenix robot (Art Robbins Instruments). Larger crystals were grown by vapor diffusion in either sitting or hanging drop trays against a reservoir containing 15−25% polyethylene glycol 3350, 175 mM NaCl, 5 mM *n*-octyl β-D-glucoside, and 100 mM sodium acetate (pH 4.6−5.6). In some cases, streak seeding was used to increase size and crystal quality.

Structure Determination. Diffraction data were collected at the Cornell High Energy Synchrotron Source (CHESS) at beamlines A1 and F2 on an ADSC Quantum 210 CCD camera. A mixture of 4 parts reservoir and 1 part ethylene glycol was used as a cryoprotectant for crystals. In soaking experiments with CcP W191G crystals, the protocol described by Goodin et al.[58] was followed. Briefly, potential small-molecule ligands were dissolved in 50% ethanol to make a 100 mM stock solution, with the exception of indole, which was dissolved in 100% ethanol. The crystals were soaked in a drop of well solution with a final ligand concentration of 30 mM for 30 s prior to soaking with cryoprotectant. Longer ligand soaks proved to be detrimental to diffraction. All data were indexed and scaled with HKL2000.[59] All structures were phased using molecular replacement in PHENIX.[60] Structures of CcP W191G were refined using CNS,[61] and all other structures were refined with the PHENIX suite.[60] Building and adjustments were made with COOT.[62] Translation/libration/screw (TLS) parameters were applied in PHENIX to model Cc anisotropic disorder in the lattice.

Saturation Kinetics. The steady-state assay for CcP peroxidase activity was performed as previously described.[63] Stock solutions of Cc were reduced on ice in the glovebox by incubation with 10 mM DTT for 1 h. DTT was then removed by buffer exchange into 100 mM KP_i (pH 6.0), either by PD-10 desalting columns or 10 rounds of concentration and dilution using Millipore Amicon Ultra centrifugal filters (10 kDa cutoff). Samples containing 2 nM peroxidase, 100 mM KP_i (pH 6.0), and 0−75 μM Cc were then prepared anaerobically in a volume of 1800 μL in gastight cuvettes (StarnaCell). Samples were placed in a Hewlett-Packard 8909A Peltier sample cooler kept at 24 °C and stirred at 500 rpm. Spectra were recorded with an Agilent 8453 spectrophotometer. Samples were blanked prior to data acquisition to monitor the change in absorbance over time. The reaction was initiated by addition of hydrogen peroxide to a final concentration of 170 μM. Oxidation of Cc was monitored at 550 and 540 nm, and a constant baseline was set by normalizing to the absorbance at 750 nm. The kinetics were monitored for 60 s, with data collected every 0.5 s. The initial range of data in which the reaction progress is linear was chosen to represent the steady-state progress of the reaction, where the Cc concentration greatly exceeded the enzyme concentration. A linear fit was applied to this range, and the slope was taken as the reaction velocity (v_0) for that concentration. For every concentration of Cc, three samples were measured.

For measuring the effect of potential ligands on CcP activity, stock solutions of the ligands were prepared in 50% ethanol, or 100% ethanol in the case of indole. Samples were prepared as described above, with a Cc concentration of 30 μM, a ligand concentration of 2 mM, and a final ethanol concentration of <10 mM. To determine Michaelis−Menten constants V_{max} and K_M, the average v_0 was plotted versus concentration and fit to the equation $v = (V_{max}[Cc])/(K_M + [Cc])$ in Mathematica.[64] Steady-state parameters of W191G with ligands were compared to those of W191F with ligands to identify effects not attributable to cavity binding.

Cpd I Spectroscopic Characterization. For UV/vis spectroscopy, 30 μM CcP was prepared in 100 mM KP_i (pH 6.0), and hydrogen peroxide was added to a final concentration of 1 mM. Stock solutions were diluted in 100 mM KP_i (pH 6.0) to 1−4 μM for recording optical spectra on an Agilent 8453 spectrophotometer. For continuous wave EPR spectrosopy, CcP was prepared at a concentration of ∼0.5 mM to obtain stronger signals. Prior to data collection, samples were diluted into a buffer of 100 mM KP_i (pH 6.0), 2 mM hydrogen peroxide, and 30% glycerol. Samples were loaded into EPR tubes, flash-frozen minutes after addition of hydrogen peroxide, and measured with a Bruker EleXSys II spectrometer at 9 GHz with a 1.5 G modulation amplitude, a 100 kHz modulation frequency, and a 25−30 dB microwave attenuation.

The L-tyrosine EPR standard was prepared as described previously.[65] L-Tyrosine was dissolved in a sodium borate buffer (pH 10), degassed via three freeze−thaw cycles, and flame-

DOI: 10.1021/acs.biochem.6b00262
Biochemistry 2016, 55, 4807−4822

Table 1. Diffraction Data Collection and Structure Refinement Statistics

	W191F	W191Y	W191G	W191G with aniline
		Data Collection		
space group	$P2_1$	$P2_1$	$P2_1$	$P2_1$
a, *b*, *c* (Å)	44.8, 113.8, 88.2	45.5, 110.2, 88.2	45.4, 117.1, 88.9	45.4, 110.3, 87.9
β (deg)	105.3	104.3	105.1	105.5
no. of unique reflections	51828	21533	52508	27854
resolution (Å)	2.01	2.4	2.06	2.5
last shell resolution[a] (Å)	2.03−2.01	2.44−2.40	2.13−2.06	2.54−2.5
completeness (%)	92.2/90.7	80.7/51.1	96.1/98.3	95.9/98.0
I/σ	14.9/3.8	8.4/2.0	9.2/2.7	7.3/2.0
R_{merge}[b]	0.222/0.488	0.135/0.670	0.121/0.46	0.158/0.537
		Refinement		
R_{work}[c] (%)	21.5/23.4	22.3/28.9	28.1/33.8	25.0/31.1
R_{free}[c] (%)	26.7/37.6	30.9/43.9	29.7/34.6	29.4/43.5
no. of atoms	7052	6560	6912	6657
no. of water molecules	534	40	324	55
mean *B* value (Å^2)	33.6	70.5	43.3	66.4
B value (waters) (Å^2)	35.9	55.4	44.3	52.0
B value (ligand) (Å^2)	NA	NA	NA	59.9
rmsd for bonds (Å)	0.004	0.003	0.003	0.003
rmsd for angles (deg)	0.8	0.7	0.8	1.0
ϕ/ψ stats (%)				
most favored	97.6	94.5	96.8	96.1
outliers	0.13	0.25	0.25	0.0
Protein Data Bank entry	5CIF	5CIH	5CIG	5CIE

	W191G with *o*-toluidine	W191G with 24dma	W191G with 3abt
	Data Collection		
space group	$P2_1$	$P2_1$	$P2_1$
a, *b*, *c* (Å)	45.4, 111.9, 87.9	45.4, 107.5, 87.2	45.3, 117.5, 88.5
β (deg)	104.3	104.5	104.4
no. of unique reflections	20376	15317	51366
resolution (Å)	2.76	3.0	2.10
last shell resolution[a] (Å)	2.59−2.76	3.05−3.00	2.14−2.10
completeness (%)	93.5/65.7	95.9/85.0	98.7/90.0
I/σ	17.1/3.2	17.2/3.4	14.2/4.7
R_{merge}[b]	0.092/0.388	0.123/0.512	0.096/0.402
	Refinement		
R_{work}[c] (%)	21.4/26.9	23.5/27.8	19.2/24.8
R_{free}[c] (%)	26.8/34.8	31.3/37.8	22.8/29.1
no. of atoms	6613	6606	7076
no. of water molecules	9	0	496
mean *B* value (Å^2)	70.2	60.1	45.2
B value (waters) (Å^2)	54.4	NA	45.7
B value (ligand) (Å^2)	76.3	57.5	46.3
rmsd for bonds (Å)	0.005	0.003	0.005
rmsd for angles (deg)	1.0	0.8	0.9
ϕ/ψ stats (%)			
most favored	95.7	94.0	98.6
outliers	0.38	0.31	0.25
Protein Data Bank entry	5CID	5CIB	5CIC

[a]Highest-resolution range for compiling statistics. [b]$R_{merge} = (\sum_i\sum_j|I_j - \langle I_i\rangle|)/[\sum_i(\sum_j I_j)]$, where I_j is the intensity of the *j*th observation of reflection *i*, $\langle I_i\rangle$ is the average intensity of reflection *i*, and N_i is the redundancy of reflection *i*. [c]R_{work} or $R_{free} = (\sum|F_{obs} - F_{calc}|)/(\sum|F_{obs}|)$.

sealed in a quartz EPR tube. While frozen in liquid nitrogen in a finger dewar, the sample was irradiated with a 600 W mercury lamp for 3−4 min to generate the free tyrosyl radical.

CcP Turnover Experiments. Following the method used for W191F,[66] Cc(II) was reduced with dithionite and buffer exchanged into 100 mM KP_i (pH 6). While the sample was being continuously stirred at 25 °C, 4 μM H_2O_2 was added to 2 μM CcP and 30 μM reduced Cc in 100 mM KP_i (pH 6), bringing the total volume to 1800 μL. Spectral changes were monitored at 550, 540, and 434 nm over 15 min with a single baseline set at 800 nm. The change in Cc(II) concentration was determined spectrally by monitoring $A_{550} - A_{540}$ and applying an extinction coefficient of 19.2 mM^{-1} cm^{-1}. Traces were fitted to a monoexponential equation using MATLAB (The MathWorks, Inc., Natick, MA)

DOI: 10.1021/acs.biochem.6b00262
Biochemistry 2016, 55, 4807−4822

$$y = a\{1 - \exp[-k_{obs}(x - t_0)]\} + y_0$$

The offset t_0 for the early phase was determined by an immediate drop in $A_{550} - A_{540}$ after addition of peroxide. For the slow phase, the offset was established at the maximum of A_{434}. Traces were truncated from the onset of the early phase to the onset of the slow phase to obtain k_{obs} for the early phase. The k_{obs} for the latter phase was determined from data truncated from the onset of the slow phase to 40 s later. To determine the minimal amount of peroxide required for CcP ferryl generation, 8 μM CcP in 100 mM KP_i (pH 6) was titrated with 8−24 μM H_2O_2 and the reaction monitored at 434 nm. Once formed, the CcP ferryl was stable for at least 2 h on ice. The H_2O_2 concentration was determined by titration with permanganate. Stock peroxide was diluted 10-fold, and 1 mL was combined with approximately 30 mL of water and 10 mL of 3 M sulfuric acid. While the sample was being stirred, a 0.025 M solution of $KMnO_4$ was added by buret until the midpoint was observed. The concentration of H_2O_2 was calculated from the volume dispensed. For multiple-turnover experiments, Cc(II) was reduced with dithionite and buffer exchanged into 100 mM KP_i (pH 6). While the sample was being continuously stirred at 25 °C, 5−10 μM H_2O_2 was added to 1 μM CcP and 30 μM reduced Cc in 100 mM KP_i (pH 6), bringing the total volume to 1800 μL. Initial rate values were determined by fitting the data to a monoexponential decay and then taking the first derivative at time zero. For examination by cw EPR, reduced Cc and CcP W191Y were combined in a 15:1 ratio, with the final concentration of CcP being ∼0.2 mM in a buffer of 100 mM KP_i (pH 6) and 25% glycerol. H_2O_2 was added to a final concentration of ∼0.4 mM, and the solution was rapidly mixed by stirring or vortexing. At 30 and 60 s, ∼70 μL of sample was transferred to an X-band EPR tube and flash-frozen in liquid nitrogen. Data were collected as described above.

Transient Absorption Spectroscopy. All preparations of spectroscopic samples were conducted under anaerobic conditions to avoid quenching of ^{3}ZnCcP by oxygen. ZnCcP was diluted into 10 or 100 mM KP_i (pH 7.0) to a concentration of 100−200 μM and combined with Fe(III)Cc in a 1:2 molar ratio. Drops (4 μL) were placed on siliconized glass coverslips (Hampton) and glued to glass slides using a ring of epoxy to form a gastight seal, with an average path length of ∼0.5 mm. Samples were placed in the path of a probe light, provided by a 75 W Xe-arc lamp. Excitation light was provided either by an Opotek Opolette Nd:YAG laser tuned to 560 nm with approximately 2 mJ of power per 8 ns pulse or by a Continuum Surelight Nd:YAG laser providing light at 532 nm at approximately 5 mJ of power per 4 ns pulse. The fluorescent efficiency at various excitation wavelengths was measured by tracking the light emitted at 600 nm. Samples were preferentially excited in the Q-bands at 560 nm, although there was also sufficient cross section at 532 nm for sample excitation. The two excitation energies produced identical kinetics, with both lasers firing at 20 Hz. Exposure to excitation light was controlled by a Hamamatsu A6538 Optical Laser shutter, and the absorbance of the probe light was measured with a Hamamatsu Photonic Multichannel Analyzer (PMA). Unless otherwise specified, spectra recorded by the PMA were acquired from a 1−50 μs exposure time and averaged 20−200 times, depending on the strength of the signal. The laser Q-switch firing acted as the master trigger, with a Digital Delay Generator DG355 (Stanford Research Systems) controlling timing between the other elements. Detection of scattered laser light set t_0 (time = 0 s). Subsequent time points were then sampled randomly with an entire UV/vis spectrum collected for each exposure. The time delay points were acquired in a random order to mitigate the effects of any photobleaching during data collection. To record a given time point, N reference spectra were recorded at the specified delay time (relative to t_0), where N is the number of spectra being averaged. Next, the laser shutter opened, and N excited spectra were recorded at the same delay. Difference spectra were calculated as ΔA = log(excited/reference), accumulated, and averaged over N.

To process the data, data vectors across the wavelength range were reordered in time and subjected to global analysis by Glotaran.[67] Data below 375 nm were discarded because little light at those wavelengths was transmitted through the optics to the PMA, and data above 750 nm were discarded because of a lack of spectral features. A baseline correction at the triplet-state isosbestic point of 546 nm was applied.[17] Single-value decomposition (SVD) of the multiwavelength data was conducted to reconstruct the minimal number of spectroscopic (difference) states sufficient to describe the kinetic progress. In general, sequential reaction kinetics were assumed, and as such, single- or double-exponential terms were used to connect the spectroscopic states in time.

RESULTS

In the following experiments, CcP Trp191 was substituted with Phe,[68] Gly,[48] and Tyr. For the W191G variant, a series of small molecules were also introduced into the cavity created by removal of the residue 191 side chain. In all cases, crystal structures of the CcP:Cc complexes were determined to aid interpretation of reactivity data. We then examined the peroxidase activity of the variants, their ability to form Cpd I, and their photoinduced ET reactions in the context of ZnCcP:Cc.

Structures of W191(Y,F,G) CcP. The structures of W191(Y,F,G) CcP in complex with Fe(III)Cc were determined at resolutions that ranged from 2.0 to 2.4 Å (Table 1). For each of the variants, both CcP and Cc retained conformations nearly identical to those seen in the WT complex (Figure 2). In the absence of Cc, the W191G substitution causes enhanced flexibility in the 190−195 loop.[69] Because this loop resides at the binding interface with Cc, there was concern that increased flexibility would impact the formation of the crystal complex. Nonetheless, W191G binds Cc in the expected position. The two copies of the CcP:Cc complex in the asymmetric unit are very similar to each other in structure (designated as chains A and C for CcP and chains B and D for Cc). Several of the Cc moieties were not well ordered in the complex structures. As observed previously,[18] the interfaces between CcP and Cc are generally well-defined, but electron density weakens at the periphery of the complexes, largely because of Cc conformational variability within the lattice. This disorder is difficult to model well and somewhat degrades the refinement statistics relative to those expected for an average structure of similar resolution (Table 1).

In the CcP:Cc complexes, the altered side chains of W191F and W191Y occupy nearly the same position as W191 in the WT (Figure 2B), with the phenol group of W191Y and the phenyl group of W191F aligning with the imidazole of His175, which coordinates the heme and hydrogen bonds to Asp235.[70] There is no polar moiety within hydrogen bonding range of the Tyr191 hydroxyl group (Figure 2B) (the Thr180 side chain is

DOI: 10.1021/acs.biochem.6b00262
Biochemistry 2016, 55, 4807−4822

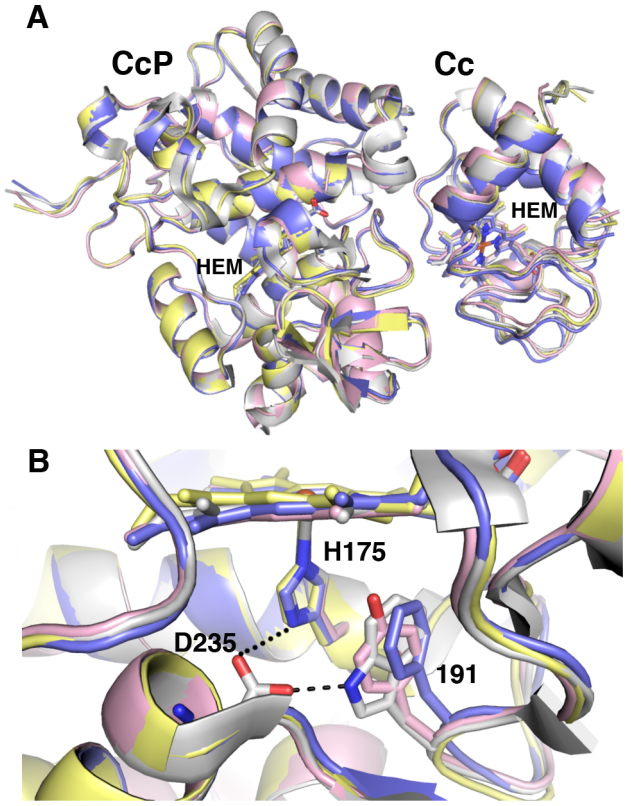

Figure 2. Structures of CcP W191X variants with Cc. (A) Overlay of the CcP:Cc W191X structures with the WT complex showing a high degree of similarity (WT, Protein Data Bank entry 1U74, in white, W191Y in pink, W191F in blue, and W191G in yellow). One of the two unique complexes in the asymmetric unit is shown. (B) Superposition of residue 191 in the respective crystal structures showing that the aromatic side chains all hold approximately the same position in each variant, with each side chain oriented in the plane of coordinating His175. In WT CcP, Trp191 hydrogen bonds with Asp235. The side chains of Tyr191 and Phe191 have no polar contacts. The peptide backbone of Gly191 has the same conformation that Trp191 in WT does.

within 3.3 Å of the Tyr191 hydroxyl group, but the hydroxyl group hydrogen bonds with the backbone of Gly189). Instead, the Tyr191 hydroxyl proton may be stabilized by the π-electrons of the heme itself. In the W191G Cc complex, difference electron density confirms the presence of ordered water molecules in the cavity created by the loss of the W191 indole. However, the water positions differ somewhat from those of uncomplexed CcP[48,49] and vary between chain A and chain C in these structures. No ordered water molecules were detected near the side chains of Tyr191 or Phe191 in the respective structures.

Complementation of the W191G Pocket with Small Molecules. To promote ligand binding in the W191G cavity, crystals were soaked with several redox-active compounds at concentrations of 30 mM (Figure 3). These compounds were selected considering their structural similarity to aniline or indoline, each of which is a ligand demonstrated to bind the pocket that has a solution redox potential similar to that of Trp.[71,72] Although the affinities of these compounds for W191G have not been measured, we reasoned that they would be in a range similar to those found for aniline and indoline (30 and 160 μM for CcP W191G, respectively[58]). Of the compounds tested, four bound to W191G as evidenced by the presence of significant difference electron density in the cavity made vacant by the W191G substitution [$>2.0\sigma$ in a $F_o - F_c$ electron density difference map (Figure 4)]. Although the difference densities are changed relative to that seen in the water-filled cavity of W191G, they are ambiguous in each case; hence, the compounds may bind with multiple configurations (Figure 4). Despite the demonstrated affinity of indoline for the cavity, we did not observe any electron density for this compound in the crystal structures. Perhaps Cc association prevents movement of the 190–195 loop that is required for this larger ligand to access the pocket.[52,69] A barrier to access may have also prevented binding of indole and tryptophan, which were also not detected in the crystallization experiments. Cocrystallization of the complex with these ligands was also unsuccessful. Indole binding was possibly limited by its low solubility in the crystallization solutions.

Saturation Kinetics. WT CcP displayed the expected high peroxidase activity and typical Michaelis–Menten behavior (V_{max}/E_0 = 1600 ± 100 s^{-1}; K_m = 30 ± 7 μM; 100 mM KP_i) with respect to Cc concentration at 100 mM KP_i, where complicating factors from second-site binding are negligible.[20,73] (We note that the K_m value for WT is ~5 times higher than those of previous studies,[63,73,74] perhaps because of the different buffer conditions used here.) As expected,[48,66,68] W191F and W191G had little detectable peroxidase activity, above that of Cc oxidation by hydrogen peroxide alone. The steady-state rate of Cc(II) oxidation by W191F has previously been shown to be at least 10^3-fold lower than that by WT and linear for only a few seconds.[66] We found similar behavior for both W191F and W191G, with the lack of linearity making rates difficult to determine. Under our conditions, W191Y also appeared to be largely inactive. V_{max}/E_0 was only 40 ± 20 s^{-1} but also showed a peroxide dependence (see below).

To determine if the small-molecule compounds that bound in the W191G CcP cavity can rescue peroxidase activity, the rate of Cc oxidation was measured for W191G and compared to the value of W191F under the same conditions. As both W191G and W191F are inactive and Phe191 blocks the cavity, any peroxidase activity of W191G above that seen for W191F should reflect ligand binding. At ligand concentrations at least 1 order of magnitude above the measured K_D values (2 mM[58]), no detectable peroxidase activity of W191G was observed in the presence of any of the compounds listed in Figure 3. These results corroborate previous studies of W191G complementation.[48]

Species Formed upon Reaction with Peroxide. CcP compound I formation is evidenced in the UV/vis absorbance spectrum of WT and CcP W191Y by a shift in the Soret peak from 409 to 420 nm and the appearance of Q-bands characteristic of the oxo–ferryl species (Figure 5).[75] W191F also produces a similar Soret peak shift, from 409 to 420 nm, but the Q-bands are less well-defined[50,68] (Figure 5A). W191G displays the most unique spectrum with a 414 nm Soret peak for the ferric state. Although previous studies of the W191G reaction with peroxide found pronounced ferryl formation as indicated by a well-defined 414 nm Soret peak and Q-bands at 530 and 560 nm,[48,50] we find only a modest shift in the W191G Soret band to 417 nm with similarly small changes in the Q-bands (Figure 5A). The reason for this difference is unknown but could reflect the heme incorporation process during protein expression.

We also tested for the ability of WT, W191Y, and W191F to produce cw EPR spectra characteristic of aromatic residue

DOI: 10.1021/acs.biochem.6b00262
Biochemistry 2016, 55, 4807–4822

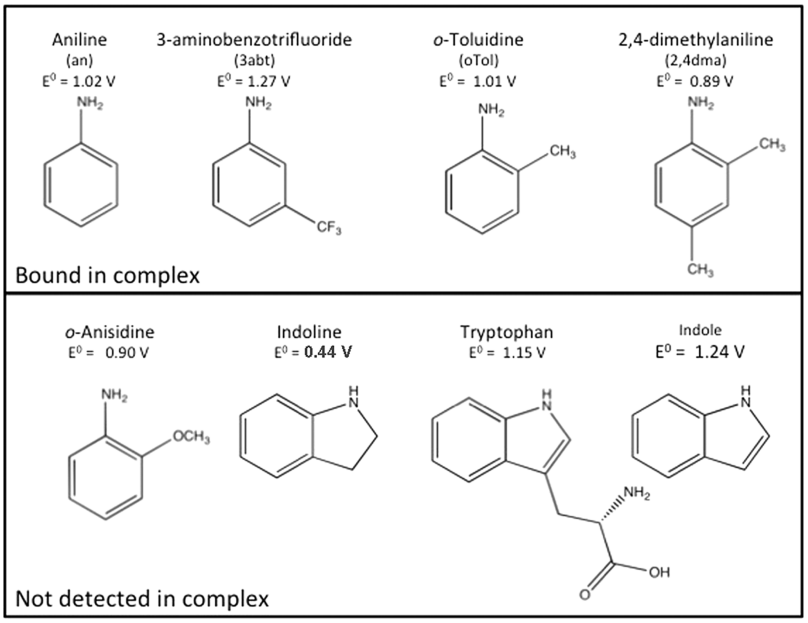

Figure 3. Compounds targeted at the W191G cavity. Compounds tested for binding W191G cavity and their respective reduction potentials (tryptophan,[110] aniline,[111] indole,[111] and aniline derivatives[90]).

oxidation (Figure 5B). As previously reported for W191G in CcP[50] and related peroxidases,[76] we observe a small amount of organic radical forms upon reaction with peroxide [$\sim^1/_{10}$ of the WT signal (Figure 5B)], presumably because of the minor oxidation of aromatic residues remote from the active center.[50,77−79] In contrast, W191Y produces a strong EPR signal characteristic of a neutral Tyr radical[80,81] with an amplitude similar to that seen with WT (Figure 5B). Thus, despite its inability to oxidize Cc(II), W191Y forms a Cpd I-like species containing an oxo−ferryl complex and a tyrosine radical. Features of the W191Y radical species correspond well with those of free tyrosyl radicals generated from UV photolysis (Figure 5B).

Oxidation of Cc(II) by W191Y Cpd I. To further investigate the inactivity of W191Y in the steady-state oxidation of Cc(II), we examined the oxidation of W191Y Cpd I by Cc(II) under pseudo-first-order conditions and compared the results to those for W191F.[66] W191F does not form a radical species at position 191 upon reaction with peroxide and exhibits only very slow turnover under steady-state conditions.[66] Titration of W191Y with hydrogen peroxide indicated that ∼2 equiv of H_2O_2 was necessary to fully form Cpd I, which was then stable for at least 5 min on ice [it is unclear why 2 equiv of H_2O_2 is needed for the initial formation of Cpd I; under multiple turnovers by W191Y, one peroxide oxidizes two Cc(II) molecules (see below)]. Following the same procedure used previously for W191F,[66] 30 μM Cc(II) was mixed with 2 μM CcP and 4 μM H_2O_2 was added to initiate the reaction, which was then monitored at 550 nm [Cc(II)], 540 nm (an isosbestic point for Cc oxidation), and 434 nm [Fe(IV)=O]. During the initial buildup of the Fe(IV)=O species at 434 nm, there was an early phase of Cc(II) oxidation with a k_1 of 0.17 ± 0.03 s^{-1}. Following the maximal absorbance at 434 nm [Fe(IV)=O peak], the oxidation of Cc(II) was monophasic (Figure 6A), giving a rate constant k_2 of 0.08 ± 0.03 s^{-1}. This behavior and value are similar to those for Cc(II) oxidation by the W191F ferryl species under analogous conditions, which also shows a slow phase of Fe(IV)=O oxidation with a k_2 of 0.14 s^{-1}.[66] Furthermore, the spectral changes at 550 nm indicate that for W191Y ∼1 equiv of Cc(II) (2.5 ± 0.5 μM) is oxidized by W191Y Cpd I on this time scale. An equivalent of Cc(II) was also oxidized during the buildup of Cpd I in the initial phase of the reaction.

We then examined multiple turnovers of Cc(II) oxidation by reacting W191Y (1 μM) with a 10-fold excess of peroxide (10 μM) and 30 μM Cc(II) (Figure 6B). The resulting reactions produced 2 equiv of oxidized Cc (22 ± 1 μM) and proceeded with a turnover number (V/E_0) of 0.29 ± 0.03 s^{-1},[1] which is greater than the rate constant for the analogous single-turnover condition (0.08 ± 0.3 s^{-1}). Notably, the amount of the ferryl species (434 nm) increases as Cc(II) decreases and then decays slowly when the peroxide is extinguished, concomitant with a small amount of Cc(II) oxidation. This behavior is somewhat different from that seen with W191F, where the CcP ferryl species remains constant until peroxide is depleted.[66] For W191F, it was suggested that the ferryl species reacts directly with peroxide to oxidize Cc(II), perhaps through the formation of additional protein-based radicals.

$$\text{Fe(IV)=O CcP} + \text{HOOH} + 2\text{Cc(II)} + 2\text{H}^+ \rightarrow \text{Fe(IV)=O CcP} + 2\text{Cc(II)} + 2\text{H}_2\text{O} \quad (5)$$

With W191Y, the ferryl appears to increase at 434 nm as the oxidation of Cc(II) slows, suggesting that in the early phase peroxide [and Cc(II)] reacts with an intermediate that precedes the ferryl in the reaction sequence. Furthermore, the multiple-turnover rate (0.29 s^{-1}) is considerably faster than the single-turnover rate (0.08 s^{-1}), and thus with excess peroxide present, the reaction is not rate-limited by oxidation of Cc(II) by Fe(IV)=O. The reaction rate did show a peroxide concentration dependence, but the relationship was complex and not proportional. Although this behavior requires further investigation, it is clear that the W191Y Cc(II) turnover rate is 10^3−10^4 times slower than that of WT CcP[82−84] because of the altered reactivity of the Tyr radical.

DOI: 10.1021/acs.biochem.6b00262
Biochemistry 2016, 55, 4807−4822

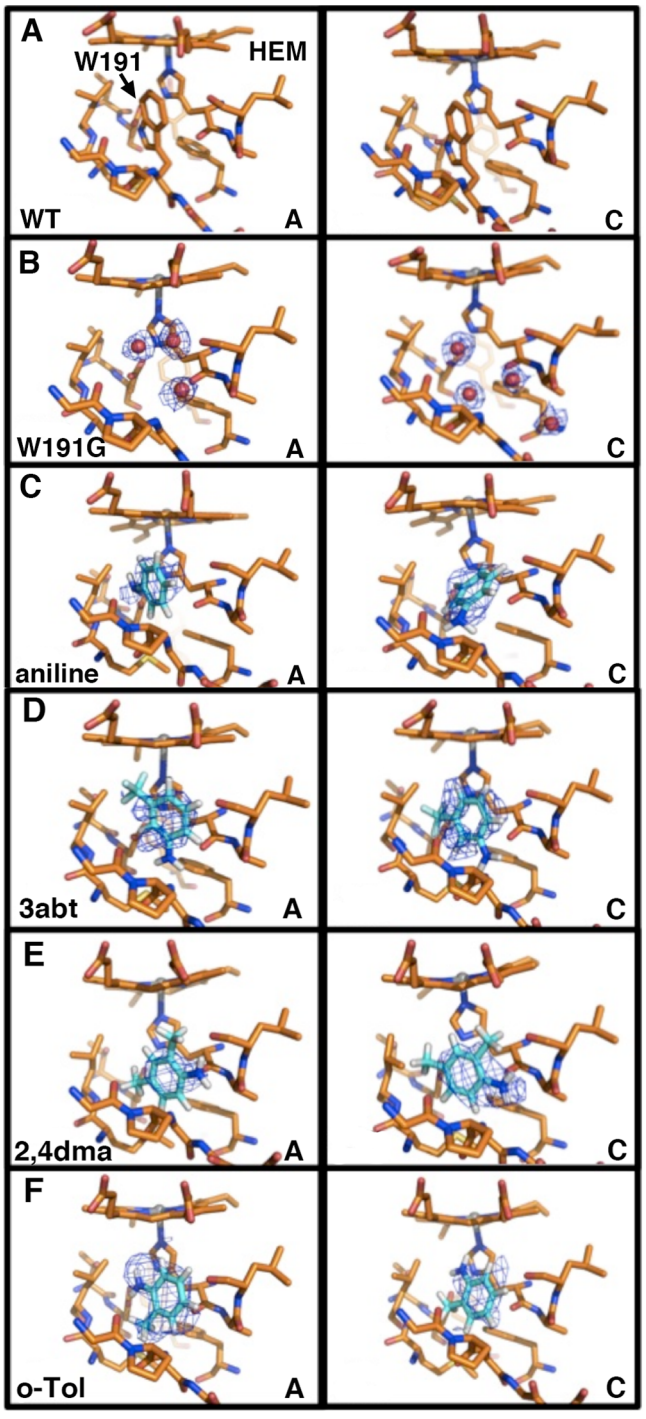

Figure 4. Ligands bound in the W191G CcP cavity. The WT CcP:Cc structure compared to the W191G CcP:Cc structure soaked with (B) nothing, (C) aniline, (D) 3-aminobenzorufluoride, (E) 2,4-dimethylaniline, and (F) *o*-toluidine. Omit map difference electron density is shown at 2.2−2.5σ for both unique complexes in the asymmetric unit (chains A and C).

Considering that W191Y does form a Tyr radical (Figure 5B), there are two possibilities for the reactivity of W191Y Cpd I. In the first case, $Y^{\bullet}$ reacts quickly to oxidize 1 equiv of Cc(II), but the remaining ferryl cannot reoxidize Y191 (as per eq 3). The second oxidation then involves reaction of the ferryl or some other intermediate with peroxide, which is fast compared to oxidation of Cc(II) by Fe(IV)=O (eq 5). In the second case, the $Y^{\bullet}$ potential is too low to oxidize Cc(II) at rates that greatly exceed the rate of oxidation by Fe(IV)=O or reaction of an intermediate state with peroxide. If the $Y^{\bullet}$ were especially stable, it may be observable during the single-turnover experiment using EPR spectroscopy. However, no $Y^{\bullet}$ was observed in the presence of Cc(II) during decay of the ferryl species (20−30 s after reaction with peroxide). Thus, the $Y^{\bullet}$ species has reacted prior to the reduction of Fe(IV)=O. Further investigation of $Y^{\bullet}$ reactivity remains to be determined by methods with better time resolution.

Photoinduced ET of ZnCcP:Cc W191 Variants. We invoked the ZnCcP:Cc system to evaluate the ability of CcP position 191 to facilitate long-range ET[2,11−16] (Figure 1). Zinc-protoporphyin IX (ZnP) provides a reactive, long-lived triplet state (^{3}ZnCcP) when excited with 532−560 nm light. In isolation, ^{3}ZnCcP will decay back to the ground state with a rate constant k_D of ∼100 s^{-1},[14,16,32,57] whereas in complex with oxidized Cc, ^{3}ZnCcP [Fe(III)Cc] is additionally quenched by heme-to-heme ET to Cc Fe(III) with rate constant k_e. The total quenching rate constant ($k_P = k_D + k_e$) is ∼260 s^{-1} for the 1:1 complex with yeast Cc, depending somewhat on ionic strength, temperature, and pH.[12,14,15,17,20,57] The resulting charge-separated state containing the ZnP cation radical (ZnP^+) and reduced Fe(II)Cc then recombines in an ET process (k_{eb}) that involves oxidation of W191 to an indole cation radical [$W^{\bullet+}$ (Figure 1)]. On the time scale of ET with Cc, the radical equilibrates extremely rapidly between ZnP and W191 or may be considered delocalized between the two centers.[3] In the WT system, k_{eb} greatly exceeds k_e, and as a result, the charge-separated intermediate forms in vanishingly small amounts. To characterize the ET reactivity of the ZnCcP:Cc complex, we employed a multichannel analyzer that allowed time resolution of complete difference spectra for the ZnCcP:Cc complex following photoexcitation. Global analysis of the data sets defined reactive states and their kinetic parameters. A typical difference spectrum for ^{3}ZnCcP in the absence of Cc is characterized by a broad, positive peak at 475 nm and two negative Q-bands at 555 and 592 nm[85] (Figure 7). A strong negative peak at 432 nm also appears, consistent with triplet excited-state spectra of isolated Zn-porphyrins.[86] The 432, 555, and 592 nm features correspond to absorption maxima in the visible spectrum of ZnCcP (Figure 7), and their diminished intensity reflects changes in the electronic state upon triplet formation.

All spectral features of ^{3}ZnCcP alone decay with a rate constant k_D of 114 ± 4 s^{-1} (Table 2). To study ET quenching of ^{3}ZnCcP by Fe(III)Cc, we used both 100 mM KP_i ionic strength conditions that favor the 1:1 complex and limit secondary binding of an additional Fe(III)Cc and 10 mM KP_i conditions that stabilize the complex against dissociation but permit some secondary-site binding.[20,57] Although, both cases potentially bring complications, we find that changes in ionic strength do not greatly alter the kinetic parameters (Table 2). Under 100 mM KP_i conditions, addition of Fe(III)Cc in 2-fold excess increases the rate constant for triplet-state decay to $k_P = k_D + k_e$ = 230 ± 12 s^{-1} (Table 2 and Figure 7). The increased level of quenching primarily results from ET to Fe(III)-Cc[14,15,32] ($k_e = k_P - k_D$ = 116 s^{-1}), which is consistent with there being little change in rate constant (<10 s^{-1}) when reduced Fe(II)Cc is added. For WT ZnCcP:Cc, the k_{eb} indeed exceeds k_e, and thus, an intermediate state could not be resolved (for individual acquisition times as low as 1 μs). Consequently, the system was best modeled with a single

DOI: 10.1021/acs.biochem.6b00262
Biochemistry 2016, 55, 4807−4822

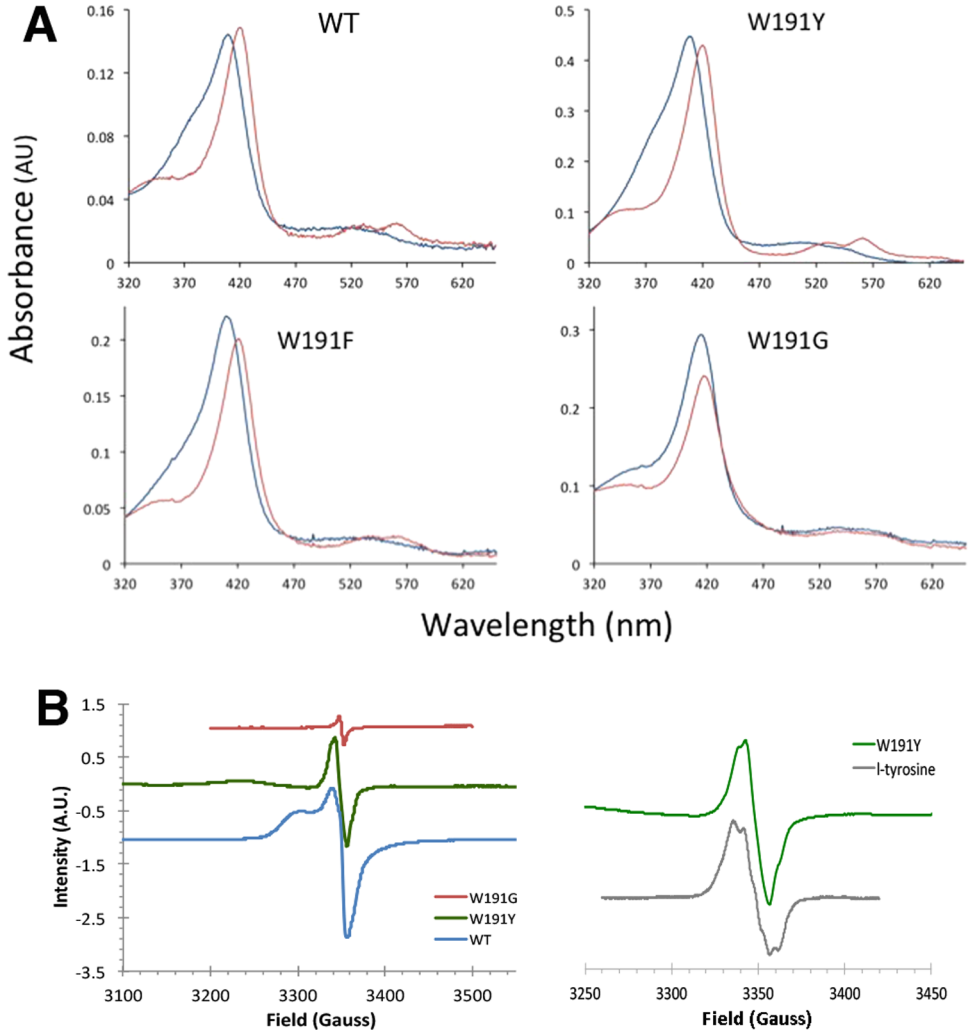

Figure 5. Compound I formation in CcP by UV/vis. (A) UV/vis spectra of CcP before (blue) and after (red) introduction of hydrogen peroxide. WT, W191F, and W191Y show the typical Soret shift from 409 to 420 nm, and Q-bands indicative of Cpd I formation. W191G shows a shift from 414 to 417 nm, with broad Q-bands that move toward those seen in WT. (B) Peroxide-induced radicals in CcP. (Left) cw EPR spectra of CcP variants with peroxide. Both WT and W191Y radical signals are much larger than those seen in W191G or W191F (not shown). A small amount of organic radical is likely formed elsewhere in W191G. Spectra recorded at X-band (9 GHz) with a 1 G modulation amplitude, a 100 kHz modulation frequency, and a 25−30 dB modulation amplitude. Data were collected at 5, 12, and 50 K for each variant; WT is shown at 5 K, W191Y at 12 K, and W191G at 50 K. Temperature has no appreciable effect on the relative amplitudes of the signals. The origin of the broad feature for W191Y at 3235 G is unknown but gives different saturation behavior and is thus distinct from the main radical signal. (Right) Neutral tyrosyl radicals were generated by UV photolysis and collected at ∼100 K. The sample exhibits similar line shape features as in W191Y.

difference spectrum corresponding to the formation and decay of ^{3}ZnCcP. The kinetic parameters (Table 2) are in line with those determined from single-wavelength measurements in other studies.[14,15,32,57]

In contrast to WT ZnCcP:Cc, W191F shows slower back ET[17,20] (Table 2). Here we resolve difference spectra for the charge-separated state [ZnP$^+$/W$^{\bullet+}$:Cc(II)]. Alone, W191F CcP produces difference spectra identical to those of WT CcP and decays uniformly at the same rate. However, in the presence of Fe(III)Cc, an additional spectral species is detected (Figure 8). At ∼10 ms, positive features begin to appear at 416, 550, and 625−690 nm. The intensities of these absorption peaks increase while the intensity of the ^{3}ZnP signal diminishes and then subsequently decay back to zero (Figure 8). Global analysis of the data reveals two distinct evolution-associated difference spectra, or EADS[87] (Figure 8), whose time-dependent linear combination effectively models the series of spectra.[87] EADS1 is identical to the triplet-state difference spectrum and fully describes the spectral features at t = 0 ms (Figure 7). EADS2 replaces EADS1 and is visible between 10 and 40 ms (Figure 8). EADS2 contains components characteristic of Fe(II)Cc (Soret peak at 416 nm and Q-bands at 522 and 550 nm) and a ZnP$^+$ π-cation radical (625−690 nm) (Figure 8) and thus represents the charge-separated state. Global analysis predicts that the Fe(II)Cc and ZnP$^+$ features rise and fall with the same kinetics. Thus, forward ET between ^{3}ZnCcP(W191F) and Fe(III)Cc produces ZnP$^+$ and Cc(II), which then recombine charge on a slower time scale (Table 2). To investigate the involvement of an additional intermediate, the data were modeled with three or more rate constants. However, any additional EADS was always degenerate to the first two and produced no new species of unique spectral quality or time evolution. Previous studies of W191F (performed at 10 mM KP$_i$) found a second slower kinetic phase for loss of ZnP$^+$:Cc(II) that results from dissociation of the complex.[17,20] The overall time scale in our experiments (40 ms) is probably

DOI: 10.1021/acs.biochem.6b00262
Biochemistry 2016, 55, 4807−4822

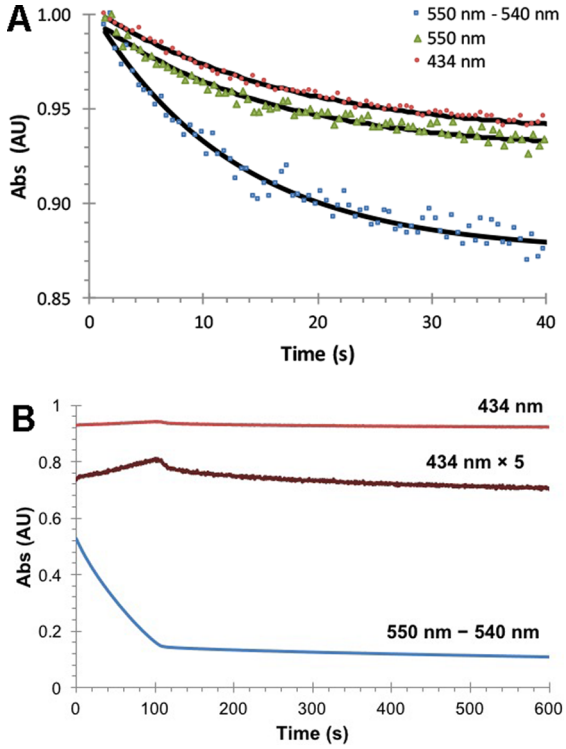

Figure 6. Oxidation of Cc(II) by W191Y. (A) Single turnover of CcP W191Y Cpd I with excess Cc(II). Reaction was initiated by mixing 4 μM H_2O_2 with 2 μM CcP W191Y and 30 μM Cc(II). After an initial phase in which Fe(IV)=O builds up at 434 nm, CcP oxidizes 1 equiv of Cc(II) with a rate constant k_2 of 0.08 ± 0.03 s^{-1}. Normalized absorbances are shown for A_{434}, A_{550}, and $A_{550} - A_{540}$. (B) Multiple turnovers of Cc(II) oxidation by CcP W191Y. Reaction was initiated by mixing 10 μM H_2O_2 with 2 μM CcP and 30 μM Cc(II). Absorbance traces are shown at 434 nm [Fe(IV)=O] and $A_{550} - A_{540}$ [Cc(II)]. In the initial phase, 22 ± 2 μM Cc(II) is consumed where the amount of Fe(IV)=O increases, until the peroxide is depleted, at which point Fe(IV)=O is slowly reduced to Fe(III) by the remaining Cc(II). The rate of the early phase is peroxide-dependent and exceeds that of Fe(IV)=O reduction in a single turnover.

too short to characterize such dissociation well, and thus, k_{eb} for intraprotein ET in the associated complex may be slightly underestimated because the system does not account for this contribution. Complex dissociation at an ionic strength of >30 mM is rapid[27] and could influence the apparent k_{eb}, especially considering that the ∼10% yield of ET products in these experiments leaves a majority of competing unreacted proteins.[20,27] We thus also investigated the reaction at a lower ionic strength (10 mM KP_i) where the W191F complex is known to be stable in the millisecond time range.[20] There was little change in the apparent rate constants between 100 and 10 mM KP_i conditions (Table 2), with both the 10 and 100 mM apparent k_{eb} values (40−70 s^{-1}) matching well with previously reported values of 40−74 s^{-1}.[17,20]

The ET behavior of ZnCcP W191G is similar to that of W191F (Table 2). ZnP^+:Cc(II) builds up and decays with similar kinetics (Figure 8); both k_e and k_{eb} are smaller than for WT but comparable to those for W191F. Thus, substitution of an aromatic group for a water-filled cavity at position 191 has an only modest effect on the apparent forward and reverse ET processes; however, weaker binding between CcP and Cc for the W191G cavity mutant may increase dissociation kinetics, which could then contribute to the slightly lower observed k_{eb}.

Tyr at position 191 does not reductively quench ^{3}ZnP because the ^{3}ZnP excited-state decay rate is unaffected in the absence of Cc. Like W191F and W191G, Cc(III) produces a modest increase in the ^{3}ZnP decay rate (Table 2), indicating quenching by ET to Cc(III). Global analysis of the transient spectra in the presence of Cc(III) reveals two major EADS, similar to that observed with W191F and W191G, with similar absorbance increases in the 625 nm range of EADS2 (Figure 8). Consequently, there is no rate acceleration for the back ET reaction in W191Y, which reacts like W191F(G) (Table 2). Like W191F, high-ionic strength (100 mM KP_i) and low-ionic strength (10 mM KP_i) conditions give very similar k_e and k_{eb} values (Table 2). Unfortunately, we were unable to study how the substituted anilines affect photoinduced ET with ZnCcP W191G because the ligands quenched ^{3}ZnP in a manner independent of binding to the W191G cavity.

DISCUSSION

Trp191 oxidation is a key feature of the CcP peroxidase mechanism and also of the ZnCcP photoinduced ET reactions. Here we report that Tyr, a similar redox-active residue at site 191, cannot support these activities, nor can a set of redox-active small molecules bound in the W191G cavity. The Tyr is unable to rescue these reactions despite the fact that it forms a stable radical adjacent to the heme upon reaction with peroxide. The influence exerted by Trp or Tyr oxidation on back ET depends on the structural and electrochemical properties of the donor, acceptor, and hopping center. Indeed, the positioning and reduction potential of a hole-hopping site must fall within certain ranges to enhance long-range ET rates.[37,45,88] When Cc(III) oxidizes ^{3}ZnP, the resulting radical is distributed between ZnP^+ and $W^{\bullet+}$, with an equilibrium weighting (K_{ex}) that depends on the difference in reduction potentials (ΔE°).

$$K_{ex} = \frac{k_f^{ex}}{k_r^{ex}} = \frac{[ZnP^0W^{\bullet+}]}{[ZnP^+W^\circ]} = e^{-F\Delta E^\circ/RT} \quad (6)$$

ET to ZnP^+ from Cc(II) could conceivably take place with and without involvement of the 191 site:

$$ZnP^\circ Cc(III) \overset{k_{eb}^1}{\leftarrow} ZnP^\circ W^{\bullet+} Cc(II) \underset{k_r^{ex}}{\overset{k_f^{ex}}{\Leftrightarrow}} ZnP^+W^\circ Cc(II)$$

$$ZnP^\circ Cc(III) \overset{k_{eb}^2}{\leftarrow} ZnP^+W^\circ Cc(II)$$

If the electron exchange reaction between ZnP^+ and W is much faster than the back electron transfer reactions (i.e., k_f^{ex}, $k_r^{ex} \gg k_{eb}^1, k_{eb}^2$) and the rate of ET to $W^{\bullet+}$ exceeds that to ZnP^+ ($k_{eb}^1 \gg k_{eb}^2$), the observed back ET rate constant (k_{obs}) will be the rate constant for transfer to $W^{\bullet+}$ weighted by the equilibrium constant for hole exchange between ZnP^+ and $W^{\bullet+}$ (eq 7).

$$k_{obs} = k_{eb}^1 K_{ex} \quad (7)$$

Known parameters justify the assumption of eq 7. ET from Cc(II) to $W^{\bullet+}$ is much faster ($k_{eb}^1 = 2 \times 10^6$ s^{-1})[8] than direct ET to ZnP^+ [$k_{eb}^2 \sim 10^1$−10^2 s^{-1} (Table 2)].[17] Thus, k_{eb}^2 sets a lower limit for any involvement of W191 to enhance ET from Cc(II). If the equilibrium constant for hole exchange $K_{ex} < 10^{-4}$ [i.e., $\Delta E^\circ > 240$ mV (eq 6)], there will be little advantage to hole hopping through the 191 site. For solution and crystalline complexes of ZnCcP with Cc(III), $k_{obs} \geq 4000$ s^{-1},[12,18,89] and thus, eq 2 implies that 120 mV < ΔE° < 180 mV. This difference in potential is consistent with measurements of the isolated moieties: $E^\circ(ZnP^\circ/ZnP^+) = 1.2$ V,[15] whereas $E^\circ(W^\circ/$

DOI: 10.1021/acs.biochem.6b00262
Biochemistry 2016, 55, 4807−4822

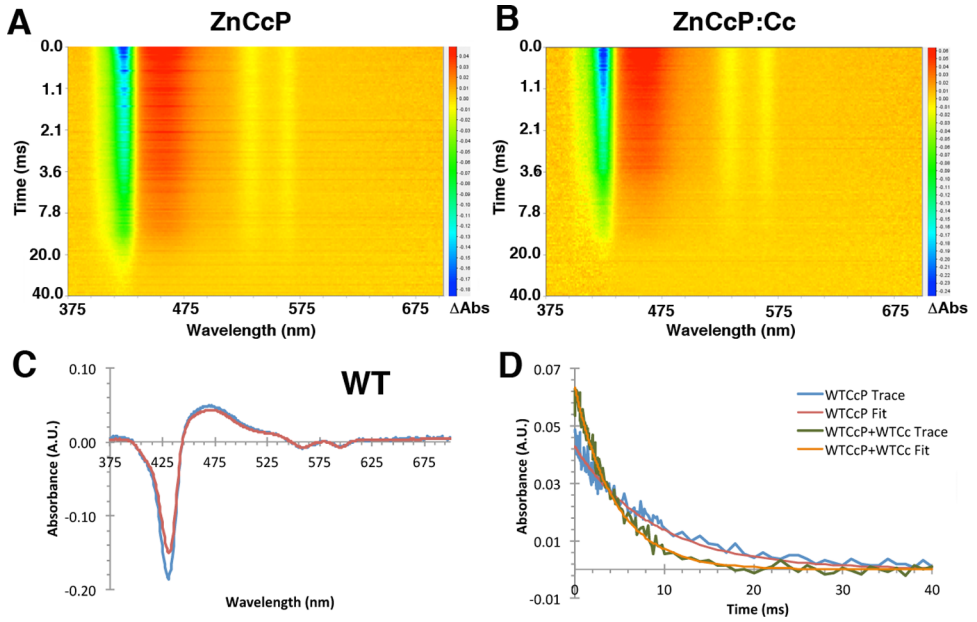

Figure 7. Time-dependent difference spectra for photoexcited ZnCcP WT with and without Cc. (A) Difference spectra for ^{3}ZnCcP decay shown as a heat map. Red, orange, and yellow colors reflect positive changes in absorption, whereas blue and green colors reflect negative changes. The difference spectrum is strongest at t = 0 ms and decays over 40 ms to a flat line. Initial time points are spaced 50 μs apart, and the time interval between successive spectra increases over the course of the measurement. The exposure time for each spectrum is 50 μs. (B) Excited-state decay of WT CcP with Fe(III)Cc added. The ^{3}ZnCcP excitation is much shorter-lived with Cc. (C) Difference spectrum of the excited state of ZnCcP at time zero. Data are colored blue, with the component state extracted from the global fit colored red. (D) Time dependence of absorbance at 475 nm for ZnCcP with and without Cc. The fit for the decay rate of the principal state in panel C is superimposed. Data shown for 100 mM KP$_i$ conditions.

Table 2. ZnCcP:Cc Photoinduced Electron Transfer Rate Constants

	k_P (s^{-1})[a]	k_D (s^{-1})[b]	k_e (s^{-1})[c]	k_{eb} (s^{-1})[d]	KP$_i$ buffer
WT	230 ± 10	114 ± 4	116 ± 13	ND[e]	100 mM
W191F	160 ± 7	102 ± 5	60 ± 10	40 ± 5	100 mM
W191F	170 ± 20	108 ± 2	60 ± 20	70 ± 10	10 mM
W191Y	200 ± 10	100 ± 2	100 ± 12	50 ± 20	100 mM
W191Y	180 ± 10	100 ± 2	80 ± 30	50 ± 10	10 mM
W191G	186 ± 10	113 ± 6	70 ± 10	16 ± 5	100 mM

[a] k_P is the ^{3}ZnP decay constant in the presence of Cc(III). [b] k_D is the ^{3}ZnP decay constant in the absence of Cc(III). [c] $k_e = k_P - k_D$ (the forward ET rate constant). [d] k_{eb} is the apparent back recombination ET rate constant. Note that under 100 mM conditions where complex dissociation may compete with back ET, k_{eb} may not be strictly first-order. [e] Not determined.

$W^{\bullet+}$) = 1.1−1.4 V.[45,81,90,91] It is worth noting that the actual reduction potentials of W191$^{\bullet+}$ and ZnP$^+$ in CcP are likely less than these values. $W^{\bullet+}$ potentials usually exceed 1 V,[45,81,90,91] and most peroxidase Cpd II [Fe(IV)=O] potentials are >0.9 V;[92,93] however, in WT CcP:Cc, the two-electron couple $E°[W^{\bullet+}Fe(IV)/W°Fe(III)] = {}^1/_2\{E°(W^{\bullet+}/W°) + E°[Fe(IV)/Fe(III)]\} = 0.740$ V.[94,95] Thus, the protein environment may substantially lower the reduction potentials of the 191 side chain and the porphyrin moiety.[96,97] Importantly, a lowered potential for $W^{\bullet+}$ is still consistent with a very small population of the charge-separated intermediate in the WT ZnCcP:Cc system. Provided that the reduction potential of the hopping site remains more than ∼200 mV higher than that of the donor Cc(II) [$E°$(Cc) = 290 mV;[98,99] i.e., ΔG = −200 mV], the standard Marcus equation[42] $\{k \sim k_{eb}(W^{\bullet+}) \exp[-(\lambda + \Delta G)^2/4\lambda kT]\}$ predicts that the back ET rate to a 191 radical will remain ∼100 times higher than the forward rate of Cc(III) reduction [$\sim 10^2$ s^{-1} (Table 2)]. [This estimate is based on a reorganization energy (λ) of ∼0.7 V for ZnCcP:Cc back ET[3] and a $k_{eb}(W^{\bullet+})$ of 2×10^6 s^{-1} for ET to W191$^{\bullet+}$ that is close to activationless.[8]]

With the crystal structure of the W191Y complex ruling out any substantial structural perturbations caused by the substitution, the inability of Tyr191 to accelerate back ET like Trp may derive from one of the two considerations mentioned previously. First, although $E°(Y^{\bullet+}/Y°)$ will likely be comparable to $E°(W^{\bullet+}/W°)$,[43,90,91,100−102] even a redox potential increase of 50−100 mV over that of Trp would decrease k^1_{eb} to the range of k^2_{eb}. Unlike Trp191, which hydrogen bonds to Asp235, there is no hydrogen bond acceptor for the Tyr hydroxyl, and thus, the Tyr redox potential may not be suitably reduced by the protein environment. In this case, during reaction of Fe(III) CcP with peroxide, Cpd I may react rapidly at $Y^{\bullet}$ or $Y^{\bullet+}$ to oxidize 1 equiv of Cc(II), but then the remaining ferryl species has insufficient potential to regenerate the Tyr radical. Oxidation of Cc(II) by the ferryl or another intermediate species would be slow relative to the reaction of this intermediate with peroxide itself. In the case of ZnCcP, the potential of ZnP$^{\bullet+}$ would also be too low to produce any appreciable amount of $Y^{\bullet}$. In the second case, the potential of neutral $Y^{\bullet}$ could be too low to oxidize Cc(II) at appreciable rates. The low pK_a of $Y^{\bullet+}$ (∼−2)[43,101] favors deprotonation to

DOI: 10.1021/acs.biochem.6b00262
Biochemistry 2016, 55, 4807−4822

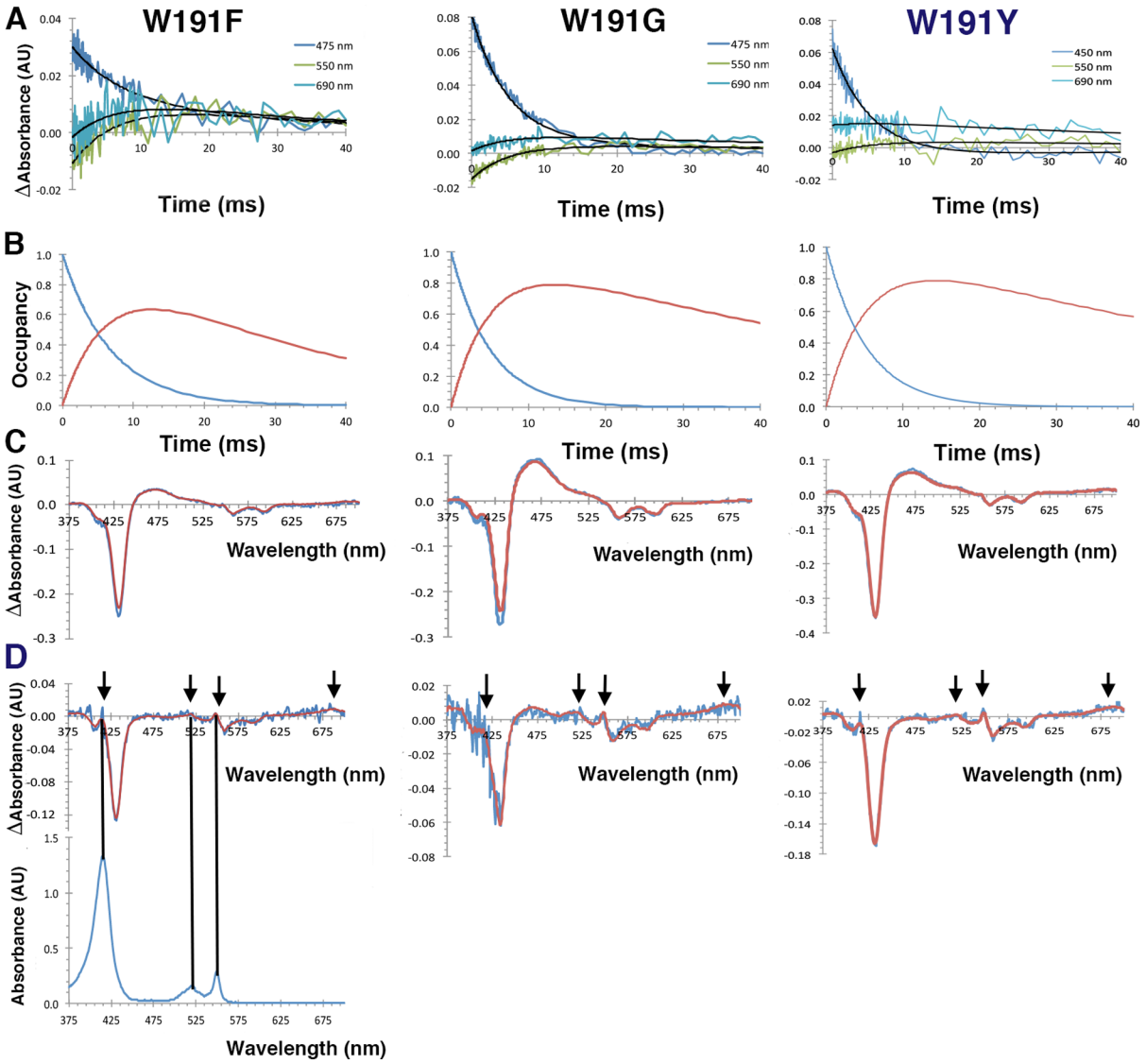

Figure 8. Detection of a charge-separated state in W191F(G) ZnCcP:Cc. (A) Time plots of the difference spectra at various wavelengths for W191F, W191G, and W191Y; 475 nm reflects ^{3}ZnP, 550 nm Cc(II), and 690 nm ZnP$^+$. (B) Progress curves for the two principal states [^{3}ZnP and ZnP$^+$:Cc(II)] defined by single-value decomposition and global analysis of the data. Traces for ^{3}ZnP are colored blue, and those for the charge-separated state are colored red (C) Difference-state spectra at t = 10 ms superimposed with the fits of the associated EADS1 for ^{3}ZnCcP. Recorded changes in absorbance are colored blue and fits red. (D) Difference-state spectra at t = 18 ms superimposed with the fits of EADS2 for the additional charge-separated intermediate in W191F, -G, and -Y. New peaks at 416 and 550 nm (arrows) correspond to Fe(II)Cc [spectra of Fe(II)Cc below], and the broad peak at ~680 nm (arrow) is characteristic of ZnP$^+$. Data shown for 100 mM KP$_i$ conditions.

the neutral radical Y$^\bullet$. The W$^{\bullet+}$ pK_a is considerably higher than this at 3.2−4.5,[103] and furthermore, the CcP heme pocket is known to stabilize the W$^{\bullet+}$ cation[104] by favorable electrostatics[96,105] and hydrogen bonding with the Asp235 carboxylate nitrogen.[96,106] In support of this scenario, during several turnovers, the ferryl species does not build up until peroxide and Cc(II) are depleted (Figure 6B), which suggests that direct reaction of peroxide with the ferryl is not rate-limiting (eq 5). However, the situation is complex and involves reaction of peroxide with something other than the ferric enzyme because the multiple-turnover rate constant is faster than the single-turnover rate constant. At this stage, we view the first scenario as more likely because reduction of Y$^\bullet$ in single-turnover experiments precedes that of the ferryl, and Y$^\bullet$ is not stable in the presence of Cc(II), albeit on relatively long time scales. Experiments with faster time resolution will help resolve this issue. The inability of the W191F and W191Y ferryl species to oxidize Cc(II) at rates comparable to that of WT CcP I supports the assertion that for WT ET proceeds primarily to the W191$^{\bullet+}$ center after it has been re-formed by reduction of Fe(IV)═O (Scheme 1).

The aniline derivatives do not rescue the peroxidase activity of the W191G CcP variant, even though they bind in the cavity and have potentials that should be in range of those of Trp. Furthermore, the pK_as of the resulting aniline cation radicals are likely higher than those of Trp and Tyr (by 2−3 pK_a units[71,103]); hence, deprotonation of the radical cations does not explain their inactivity. The inability of the ligands to hydrogen bond with the Asp235 carboxylate may prevent the protein from sufficiently lowering their reduction potentials. That said, the bound ligands have a potential range of ~0.3 V (Figure 3), and thus, at least some of them should be

DOI: 10.1021/acs.biochem.6b00262
Biochemistry 2016, 55, 4807−4822

susceptible to oxidation by ZnP^+. Thus, the more likely explanation for their inactivity stems from disorder and/or weak binding in the pocket. In particular, reorientation of the ligands in the W191G cavity, as evidenced by their heterogeneous binding configurations in the crystals, may limit interactions conducive to oxidation or destabilize any resulting radicals by promoting side reactions. Moreover, the lack of covalent attachment to the protein may short circuit hopping as the ligands exchange to solvent on the overall ET time scales. Similar results were found with the CcP Asp235Asn substitution, which destabilizes the conformation of W191 and produces Cc turnover rates similar to those of W191F.[107−109]

The near equivalence of the WT, W191Y, and W191F structures in complex with Cc lends strong support to the involvement of Trp oxidation in the charge recombination reaction. Interestingly, complete loss of the side chain in W191G produces kinetics similar to that of W191F. Even if complex dissociation is enhanced in W191G (at 100 mM KP_i), the apparent k_{eb} values are not much less than those for W191F under conditions where the complex is stable (10 mM KP_i). Thus, when hopping is inoperative, the ET rates are largely insensitive to large changes in the structure intervening between the donor and acceptor sites. Calculations suggest that although many different bonding networks contribute to electron tunneling between the porphyrin centers, those that involve Trp oxidation are the most effective at accelerating long-rang ET.[3,19] The W191F to W191G comparison supports the view that such effects are indeed large compared to those resulting from even quite substantial structural perturbations.

We conclude that a functional ET hopping site must not only meet requirements of potential and proton transfer but also maintain a degree structural stability that can be best accomplished by covalent attachment or tight binding to the protein. Moreover, there is a narrow redox potential range over which hopping will be effective at accelerating ET rates, and thus, stringent conditions must be met for multistep ET pathways to accelerate net charge transfer in proteins.

■ ASSOCIATED CONTENT

Accession Codes

Deposited in the Protein Data Bank as entries 5CIF (W191F), 5CIH (W191Y), 5CIG (W1919G), 5CIE (W191G with aniline), 5CID (W191G with toluidine), 5CIB (W191G with 24dma), and 5CIC (W191G with 3abt).

■ AUTHOR INFORMATION

Corresponding Author

*E-mail: bc69@cornell.edu. Telephone: (607) 254-8634.

Funding

Support provided by National Science Foundation Grant CHE-0749997 (B.R.C.) and Molecular Biophysics Training Grant T32GM008267 (T.M.P.) and ACERT Grant NIH/NIGMS P41GM103521.

Notes

The authors declare no competing financial interest.

■ ACKNOWLEDGMENTS

We thank the Cornell High Energy Synchrotron Source (CHESS) and the National Biomedical Center for ESR Technologies for access to data collection facilities and Nancy Li for help with protein purification. We also thank the anonymous reviewers for very useful comments in the revision of the manuscript.

■ ABBREVIATIONS

Cc, cytochrome *c*; CcP, cytochrome *c* peroxidase; Cpd I, compound I; Cpd II, compound II; cw, continuous wave; EADS, evolution-associated difference spectrum; EPR, electron paramagnetic resonance; ET, electron transfer; rmsd, root-mean-square deviation; Tris, 2-amino-2-(hydroxymethyl)-propane-1,3-diol; $W^{\bullet+}$, tryptophan radical cation; $Y^{\bullet}$, tyrosine radical; WT, wild-type protein sequence; ZnP, zinc-porphyrin.

■ REFERENCES

(1) Erman, J. E., and Vitello, L. B. (1998) Cytochrome c peroxidase: A model heme protein. *J. Biochem. Mol. Biol. 31*, 307−327.

(2) Nocek, J. M., Zhou, J. S., DeForest, S., Priyadarshy, S., Beratan, D. N., Onuchic, J. N., and Hoffman, B. M. (1996) Theory and practice of electron transfer within protein-protein complexes: Application to the multidomain binding of cytochrome c by cytochrome c peroxidase. *Chem. Rev. 96*, 2459−2489.

(3) Jiang, N., Kuznetsov, A., Nocek, J. M., Hoffman, B. M., Crane, B. R., Hu, X. Q., and Beratan, D. N. (2013) Distance-independent charge recombination kinetics in cytochrome c-cytochrome c peroxidase complexes: compensating changes in the electronic coupling and reorganization energies. *J. Phys. Chem. B 117*, 9129−9141.

(4) Millett, F., and Durham, B. (2002) Design of photoactive ruthenium complexes to study interprotein electron transfer. *Biochemistry 41*, 11315−11324.

(5) Nocek, J. M., Leesch, V. W., Zhou, J., Jiang, M., and Hoffman, B. M. (2000) Multi-domain binding of cytochrome c peroxidase by cytochrome c: Thermodynamic vs. microscopic binding constants. *Isr. J. Chem. 40*, 35−46.

(6) Millett, F., Miller, M. A., Geren, L., and Durham, B. (1995) Electron-transfer between cytochrome-c and cytochrome-c peroxidase. *J. Bioenerg. Biomembr. 27*, 341−351.

(7) Liu, R. Q., Hahm, S., Miller, M., Durham, B., and Millett, F. (1995) Photooxidation of trp-191 in cytochrome-c peroxidase by ruthenium cytochrome-c derivatives. *Biochemistry 34*, 973−983.

(8) Wang, K. F., Mei, H. K., Geren, L., Miller, M. A., Saunders, A., Wang, X. M., Waldner, J. L., Pielak, G. J., Durham, B., and Millett, F. (1996) Design of a ruthenium-cytochrome c derivative to measure electron transfer to the radical cation and oxyferryl heme in cytochrome c peroxidase. *Biochemistry 35*, 15107−15119.

(9) Mei, H. K., Wang, K. F., Peffer, N., Weatherly, G., Cohen, D. S., Miller, M., Pielak, G., Durham, B., and Millett, F. (1999) Role of configurational gating in intracomplex electron transfer from cytochrome c to the radical cation in cytochrome c peroxidase. *Biochemistry 38*, 6846−6854.

(10) Miller, M. A., Geren, L., Han, G. W., Saunders, A., Beasley, J., Pielak, G. J., Durham, B., Millett, F., and Kraut, J. (1996) Identifying the physiological electron transfer site of cytochrome c peroxidase by structure-based engineering (vol 35, pg 667, 1996). *Biochemistry 35*, 5948−5948.

(11) Zhou, J. S., Tran, S. T., McLendon, G., and Hoffman, B. M. (1997) Photoinduced electron transfer between cytochrome c peroxidase (D37K) and Zn-substituted cytochrome c: Probing the two-domain binding and reactivity of the peroxidase. *J. Am. Chem. Soc. 119*, 269−277.

(12) Wallin, S. A., Stemp, E. D. A., Everest, A. M., Nocek, J. M., Netzel, T. L., and Hoffman, B. M. (1991) Multiphasic intracomplex electron-transfer from cytochrome-c to zn cytochrome-c peroxidase - conformational control of reactivity. *J. Am. Chem. Soc. 113*, 1842−1844.

(13) Nocek, J. M., Stemp, E. D. A., Finnegan, M. G., Koshy, T. I., Johnson, M. K., Margoliash, E., Mauk, A. G., Smith, M., and Hoffman, B. M. (1991) Low-temperature, cooperative conformational transition

DOI: 10.1021/acs.biochem.6b00262
Biochemistry 2016, 55, 4807−4822

within Zn-cytochrome-c peroxidase, cytochrome-c complexes - Variation with cytochrome. *J. Am. Chem. Soc. 113*, 6822−6831.
(14) Liang, N., Kang, C. H., Ho, P. S., Margoliash, E., and Hoffman, B. M. (1986) Long-range electron-transfer from iron(II)-cytochrome-c to (zinc-cytochrome-c peroxidase)(+) within the 101 complex. *J. Am. Chem. Soc. 108*, 4665−4666.
(15) Ho, P. S., Sutoris, C., Liang, N., Margoliash, E., and Hoffman, B. M. (1985) Species specificity of long-range electron-transfer within the complex between zinc-substituted cytochrome-c peroxidase and cytochrome-c. *J. Am. Chem. Soc. 107*, 1070−1071.
(16) Ho, P. S., Hoffman, B. M., Solomon, N., Kang, C. H., and Margoliash, E. (1984) Kinetics and energetics of intramolecular electron-transfer in yeast cytochrome-c peroxidase. *Biochemistry 23*, 4122−4128.
(17) Seifert, J. L., Pfister, T. D., Nocek, J. M., Lu, Y., and Hoffman, B. M. (2005) Hopping in the electron-transfer photocycle of the 1:1 complex of Zn-cytochrome c peroxidase with cytochrome c. *J. Am. Chem. Soc. 127*, 5750−5751.
(18) Kang, S. A., and Crane, B. R. (2005) Effects of interface mutations on association modes and electron-transfer rates between proteins. *Proc. Natl. Acad. Sci. U. S. A. 102*, 15465−15470.
(19) Wallrapp, F. H., Voityuk, A. A., and Guallar, V. (2013) In-silico assessment of protein-protein electron transfer. a case study: cytochrome c peroxidase - cytochrome c. *PLoS Comput. Biol. 9*, e1002990.
(20) Page, T. R., and Hoffman, B. M. (2015) Control of cyclic photoinitiated electron transfer between cytochrome c peroxidase (W191F) and cytochrome c by formation of dynamic binary and ternary complexes. *Biochemistry 54*, 1188−1197.
(21) Bashir, Q., Volkov, A. N., Ullmann, G. M., and Ubbink, M. (2010) Visualization of the encounter ensemble of the transient electron transfer complex of cytochrome c and cytochrome c peroxidase. *J. Am. Chem. Soc. 132*, 241−247.
(22) Volkov, A. N., and van Nuland, N. A. J. (2013) Solution NMR study of the yeast cytochrome c peroxidase: cytochrome c interaction. *J. Biomol. NMR 56*, 255−263.
(23) Volkov, A. N., Worrall, J. A., Holtzmann, E., and Ubbink, M. (2006) Solution structure and dynamics of the complex between cytochrome c and cytochrome c peroxidase determined by paramagnetic NMR. *Proc. Natl. Acad. Sci. U. S. A. 103*, 18945−18950.
(24) Pelletier, H., and Kraut, J. (1992) Crystal-structure of a complex between electron-transfer partners, cytochrome-c peroxidase and cytochrome-c. *Science 258*, 1748−1755.
(25) Guo, M. L., Bhaskar, B., Li, H. Y., Barrows, T. P., and Poulos, T. L. (2004) Crystal structure and characterization of a cytochrome c peroxidase-cytochrome c site-specific cross-link. *Proc. Natl. Acad. Sci. U. S. A. 101*, 5940−5945.
(26) Liang, N., Mauk, A. G., Pielak, G. J., Johnson, J. A., Smith, M., and Hoffman, B. M. (1988) Regulation of interprotein electron-transfer by residue-82 of yeast cytochrome-c. *Science 240*, 311−313.
(27) Mei, H. K., Wang, K. F., McKee, S., Wang, X. M., Waldner, J. L., Pielak, G. J., Durham, B., and Millett, F. (1996) Control of formation and dissociation of the high-affinity complex between cytochrome c and cytochrome c peroxidase by ionic strength and the low-affinity binding site. *Biochemistry 35*, 15800−15806.
(28) Nocek, J. M., Hatch, S. L., Seifert, J. L., Hunter, G. W., Thomas, D. D., and Hoffman, B. M. (2002) Interprotein electron transfer in a confined space: Uncoupling protein dynamics from electron transfer by sol-gel encapsulation. *J. Am. Chem. Soc. 124*, 9404−9411.
(29) Nocek, J. M., Liang, N., Wallin, S. A., Mauk, A. G., and Hoffman, B. M. (1990) Low-temperature conformational transition within the Zn-cytochrome-c peroxidase, cytochrome-c electron-transfer complex. *J. Am. Chem. Soc. 112*, 1623−1625.
(30) Van de Water, K., Sterckx, Y. G. J., and Volkov, A. N. (2015) The low-affinity complex of cytochrome c and its peroxidase. *Nat. Commun. 6*, 7073.
(31) Kang, S. A., Hoke, K. R., and Crane, B. R. (2006) Solvent isotope effects on interfacial protein electron transfer in crystals and electrode films. *J. Am. Chem. Soc. 128*, 2346−2355.
(32) Kang, S. A., Marjavaara, P. J., and Crane, B. R. (2004) Electron transfer between cytochrome c and cytochrome c peroxidase in single crystals. *J. Am. Chem. Soc. 126*, 10836−10837.
(33) Liang, Z. X., Nocek, J. M., Huang, K., Hayes, R. T., Kurnikov, I. V., Beratan, D. N., and Hoffman, B. M. (2002) Dynamic docking and electron transfer between Zn-myoglobin and cytochrome b(5). *J. Am. Chem. Soc. 124*, 6849−6859.
(34) Seifert, J. L., Nocek, J. M., Hatch, S. L., and Hoffman, B. M. (2001) Study of electron transfer between cytochrome c and cytochrome c peroxidase by sol-gel encapsulation. *J. Inorg. Biochem. 86*, 425−425.
(35) Cordes, M., and Giese, B. (2009) Electron transfer in peptides and proteins. *Chem. Soc. Rev. 38*, 892−901.
(36) Cordes, M., Kottgen, A., Jasper, C., Jacques, O., Boudebous, H., and Giese, B. (2008) Influence of amino acid side chains on long-distance electron transfer in peptides: electron hopping via "stepping stones". *Angew. Chem., Int. Ed. 47*, 3461−3463.
(37) Warren, J. J., Ener, M. E., Vlcek, A., Winkler, J. R., and Gray, H. B. (2012) Electron hopping through proteins. *Coord. Chem. Rev. 256*, 2478−2487.
(38) Warren, J. J., Winkler, J. R., and Gray, H. B. (2013) Hopping maps for photosynthetic reaction centers. *Coord. Chem. Rev. 257*, 165−170.
(39) Lukacs, A., Eker, A. P., Byrdin, M., Brettel, K., and Vos, M. H. (2008) Electron hopping through the 15 A triple tryptophan molecular wire in DNA photolyase occurs within 30 ps. *J. Am. Chem. Soc. 130*, 14394−14395.
(40) Reece, S. Y., Seyedsayamdost, M. R., Stubbe, J., and Nocera, D. G. (2007) Direct observation of a transient tyrosine radical competent for initiating turnover in a photochemical ribonucleotide reductase. *J. Am. Chem. Soc. 129*, 13828−13830.
(41) Winkler, J. R., and Gray, H. B. (2014) Long-range electron tunneling. *J. Am. Chem. Soc. 136*, 2930−2939.
(42) Gray, H. B., and Winkler, J. R. (1999) Electron tunneling through proteins. *Q. Rev. Biophys. 36*, 341−372.
(43) Warren, J. J., Winkler, J. R., and Gray, H. B. (2012) Redox properties of tyrosine and related molecules. *FEBS Lett. 586*, 596−602.
(44) Warren, J. J., Herrera, N., Hill, M. G., Winkler, J. R., and Gray, H. B. (2013) Electron flow through nitrotyrosinate in Pseudomonas aeruginosa azurin. *J. Am. Chem. Soc. 135*, 11151−11158.
(45) Shih, C., Museth, A. K., Abrahamsson, M., Blanco-Rodriguez, A. M., Di Bilio, A. J., Sudhamsu, J., Crane, B. R., Ronayne, K. L., Towrie, M., Vlcek, A., Jr., Richards, J. H., Winkler, J. R., and Gray, H. B. (2008) Tryptophan-accelerated electron flow through proteins. *Science 320*, 1760−1762.
(46) Takematsu, K., Williamson, H., Blanco-Rodriguez, A. M., Sokolova, L., Nikolovski, P., Kaiser, J. T., Towrie, M., Clark, I. P., Vlcek, A., Winkler, J. R., and Gray, H. B. (2013) Tryptophan-accelerated electron flow across a protein-protein interface. *J. Am. Chem. Soc. 135*, 15515−15525.
(47) Giese, B., Napp, M., Jacques, O., Boudebous, H., Taylor, A. M., and Wirz, J. (2005) Multistep electron transfer in oligopeptides: direct observation of radical cation intermediates. *Angew. Chem., Int. Ed. 44*, 4073−4075.
(48) Fitzgerald, M. M., Churchill, M. J., McRee, D. E., and Goodin, D. B. (1994) Small molecule binding to an artificially created cavity at the active site of cytochrome c peroxidase. *Biochemistry 33*, 3807−3818.
(49) Musah, R. A., Jensen, G. M., Bunte, S. W., Rosenfeld, R. J., and Goodin, D. B. (2002) Artificial protein cavities as specific ligand-binding templates: Characterization of an engineered heterocyclic cation-binding site that preserves the evolved specificity of the parent protein. *J. Mol. Biol. 315*, 845−857.
(50) Musah, R. A., and Goodin, D. B. (1997) Introduction of novel substrate oxidation into cytochrome c peroxidase by cavity complementation: Oxidation of 2-aminothiazole and covalent modification of the enzyme. *Biochemistry 36*, 11665−11674.

DOI: 10.1021/acs.biochem.6b00262
Biochemistry 2016, 55, 4807−4822

(51) Cao, Y., Musah, R. A., Wilcox, S. K., Goodin, D. B., and McRee, D. E. (1998) Protein conformer selection by ligand binding observed with crystallography. *Protein Sci. 7*, 72−78.
(52) Hays Putnam, A.-M. A., Lee, Y. T., and Goodin, D. B. (2009) Replacement of an electron transfer pathway in cytochrome c peroxidase with a surrogate peptide. *Biochemistry 48*, 1−3.
(53) Panavas, T., Sanders, C., and Butt, T. R. (2009) SUMO fusion technology for enhanced protein production in prokaryotic and eukaryotic expression systems. In *SUMO Protocols*, pp 303−317, Springer, Dordrecht, The Netherlands.
(54) Pollock, W. B. R., Rosell, F. I., Twitchett, M. B., Dumont, M. E., and Mauk, A. G. (1998) Bacterial expression of a mitochondrial cytochrome c. Trimethylation of Lys72 in yeast iso-1-cytochrome c and the alkaline conformational transition. *Biochemistry 37*, 6124−6131.
(55) Teske, J. G., Savenkova, M. I., Mauro, J. M., Erman, J. E., and Satterlee, J. D. (2000) Yeast cytochrome c peroxidase expression in Escherichia coli and rapid isolation of various highly pure holoenzymes. *Protein Expression Purif. 19*, 139−147.
(56) Yonetani, T. (1967) Studies on cytochrome c peroxidase X. Crystalline apo-and reconstituted holoenzymes. *J. Biol. Chem. 242*, 5008−5013.
(57) Stemp, E. D. A., and Hoffman, B. M. (1993) Cytochrome-c peroxidase binds 2 molecules of cytochrome-c - evidence for a low-affinity, electron-transfer-active site on cytochrome-c peroxidase. *Biochemistry 32*, 10848−10865.
(58) Musah, R. A., Jensen, G. M., Bunte, S. W., Rosenfeld, R. J., and Goodin, D. B. (2002) Artificial protein cavities as specific ligand-binding templates: characterization of an engineered heterocyclic cation-binding site that preserves the evolved specificity of the parent protein. *J. Mol. Biol. 315*, 845−857.
(59) Otwinowski, A., and Minor, W. (1997) Processing of X-ray diffraction data in oscillation mode. *Methods Enzymol. 276*, 307−325.
(60) Adams, P. D., Afonine, P. V., Bunkoczi, G., Chen, V. B., Davis, I. W., Echols, N., Headd, J. J., Hung, L.-W., Kapral, G. J., Grosse-Kunstleve, R. W., et al. (2010) PHENIX: a comprehensive Python-based system for macromolecular structure solution. *Acta Crystallogr., Sect. D: Biol. Crystallogr. 66*, 213−221.
(61) Brunger, A. T., Adams, P. D., Clore, G. M., Delano, W. L., Gros, P., Grosse-Kunstleve, R. W., Jiang, J. S., Kuszewski, J., Nilges, M., Pannu, N. S., Read, R. J., Rice, L. M., Simonson, T., and Warren, G. L. (1998) Crystallography and NMR system: a new software suite for macromolecular structure determination. *Acta Crystallogr., Sect. D: Biol. Crystallogr. 54*, 905−921.
(62) Emsley, P., and Cowtan, K. (2004) Coot: model-building tools for molecular graphics. *Acta Crystallogr., Sect. D: Biol. Crystallogr. 60*, 2126−2132.
(63) Kang, C. H., Ferguson-Miller, S., and Margoliash, E. (1977) Steady state kinetics and binding of euakryotic cytochromes c with yeast cytochrome c peroxidase. *J. Biol. Chem. 252*, 919−926.
(64) English, B. P., Min, W., van Oijen, A. M., Lee, K. T., Luo, G., Sun, H., Cherayil, B. J., Kou, S., and Xie, X. S. (2006) Ever-fluctuating single enzyme molecules: Michaelis-Menten equation revisited. *Nat. Chem. Biol. 2*, 87−94.
(65) Barry, B. A., El-Deeb, M. K., Sandusky, P. O., and Babcock, G. T. (1990) TYrosine radicals in photosystem ii and related model compounds characterization by isotopic labeling and epr spectroscopy. *J. Biol. Chem. 265*, 20139−20143.
(66) Miller, M. A., Vitello, L., and Erman, J. E. (1995) Regulation of interprotein electron-transfer by trp-191 of cytochrome-c peroxidase. *Biochemistry 34*, 12048−12058.
(67) Snellenburg, J. J., Laptenok, S. P., Seger, R., Mullen, K. M., and van Stokkum, I. H. M. (2012) Glotaran: A Java-Based Graphical User Interface for the R Package TIMP. *Journal of Statistical Software 49*, 1−22.
(68) Erman, J. E., Vitello, L. B., Mauro, J. M., and Kraut, J. (1989) Detection of an oxyferryl porphyrin pi-cation-radical intermediate in the reaction between hydrogen-peroxide and a mutant yeast cytochrome-c peroxidase - Evidence for tryptophan-191 involvement in the radical site of compound-I. *Biochemistry 28*, 7992−7995.
(69) Fitzgerald, M. M., Musah, R. A., McRee, D. E., and Goodin, D. B. (1996) A ligand-gated, hinged loop rearrangement opens a channel to a buried artificial protein cavity. *Nat. Struct. Biol. 3*, 626−631.
(70) Finzel, B. C., Poulos, T. L., and Kraut, J. (1984) Crystal structure of yeast cytochrome c peroxidase refined at 1.7-A resolution. *J. Biol. Chem. 259*, 13027−13036.
(71) Yu, A., Liu, Y. H., Li, Z. C., and Cheng, J. P. (2007) Computation of pK(a) values of substituted aniline radical cations in dimethylsulfoxide solution. *J. Phys. Chem. A 111*, 9978−9987.
(72) DeFelippis, M. R., Murthy, C. P., Faraggi, M., and Klapper, M. H. (1989) Pulse radiolytic measurement of redox potentials: the tyrosine and tryptophan radicals. *Biochemistry 28*, 4847−4853.
(73) Miller, M. A. (1996) A complete mechanism for steady-state oxidation of yeast cytochrome c by yeast cytochrome c peroxidase. *Biochemistry 35*, 15791−15799.
(74) Volkov, A. N., Bashir, O., Worrall, J. A. R., and Ubbink, M. (2009) Binding hot spot in the weak protein complex of physiological redox partners yeast cytochrome c and cytochrome c peroxidase. *J. Mol. Biol. 385*, 1003−1013.
(75) Yonetani, T. (1965) Studies on Cytochrome c Peroxidase II. Stoichiometry Between Enzyme, H_2O_2, and ferrocytochrome c and enzymic determination of extinction coefficients of cytochrome c. *J. Biol. Chem. 240*, 4509−4514.
(76) Jasion, V. S., Polanco, J. A., Meharenna, Y. T., Li, H. Y., and Poulos, T. L. (2011) Crystal structure of leishmania major peroxidase and characterization of the compound I tryptophan radical. *J. Biol. Chem. 286*, 24608−24615.
(77) Ivancich, A., Dorlet, P., Goodin, D. B., and Un, S. (2001) Multifrequency high-field EPR study of the tryptophanyl and tyrosyl radical intermediates in wild-type and the W191G mutant of cytochrome c peroxidase. *J. Am. Chem. Soc. 123*, 5050−5058.
(78) Miner, K. D., Pfister, T. D., Hosseinzadeh, P., Karaduman, N., Donald, L. J., Loewen, P. C., Lu, Y., and Ivancich, A. (2014) Identifying the elusive sites of tyrosyl radicals in cytochrome c peroxidase: implications for oxidation of substrates bound at a site remote from the heme. *Biochemistry 53*, 3781−3789.
(79) Bernini, C., Arezzini, E., Basosi, R., and Sinicropi, A. (2014) In Silico Spectroscopy of tryptophan and tyrosine radicals involved in the long-range electron transfer of cytochrome c peroxidase. *J. Phys. Chem. B 118*, 9525−9537.
(80) Debus, R. J., Barry, B. A., Babcock, G. T., and McIntosh, L. (1988) Site-directed mutagenesis identifies a tyrosine radical involved in the photosynthetic oxygen-evolving system. *Proc. Natl. Acad. Sci. U. S. A. 85*, 427−430.
(81) Wehbi, W. A., Di Bilio, A. J., Crane, B. R., Winkler, J. R., and Gray, H. B. (2001) Properties of photogenerated aromatic side-chain radicals in rhenium-modified copper proteins. *J. Inorg. Biochem. 86*, 477−477.
(82) Hazzard, J. T., Poulos, T. L., and Tollin, G. (1987) Kinetics of reduction by free flavin semiquinones of the components of the cytochrome-c-cytochrome-c peroxidase complex and intracomplex electron-transfer. *Biochemistry 26*, 2836−2848.
(83) Miller, M. A., Hazzard, J. T., Mauro, J. M., Edwards, S. L., Simons, P. C., Tollin, G., and Kraut, J. (1988) Site-directed mutagenesis of yeast cytochrome-c peroxidase shows histidine-181 is not required for oxidation of ferrocytochrome-c. *Biochemistry 27*, 9081−9088.
(84) Liu, R. Q., Miller, M. A., Han, G. W., Hahm, S., Geren, L., Hibdon, S., Kraut, J., Durham, B., and Millett, F. (1994) Role of methionine-230 in intramolecular electron-transfer between the oxyferryl heme and tryptophan-191 in cytochrome-c peroxidase compound-II. *Biochemistry 33*, 8678−8685.
(85) Koloczek, H., Horie, T., Yonetani, T., Anni, H., Maniara, G., and Vanderkooi, J. (1987) Interaction between cytochrome c and cytochrome c peroxidase: excited-state reactions of zinc-and tin-substituted derivatives. *Biochemistry 26*, 3142−3148.

DOI: 10.1021/acs.biochem.6b00262
Biochemistry 2016, 55, 4807−4822

(86) Walters, V. A., Depaula, J. C., Jackson, B., Nutaitis, C., Hall, K., Lind, J., Cardozo, K., Chandran, K., Raible, D., and Phillips, C. M. (1995) Electronic-structure of triplet-states of zinc(II) tetraphenylporphyrins. *J. Phys. Chem. 99*, 1166−1171.
(87) van Stokkum, I. H., Larsen, D. S., and van Grondelle, R. (2004) Global and target analysis of time-resolved spectra. *Biochim. Biophys. Acta, Bioenerg. 1657*, 82−104.
(88) Page, C. C., Moser, C. C., Chen, X. X., and Dutton, P. L. (1999) Natural engineering principles of electron tunnelling in biological oxidation-reduction. *Nature 402*, 47−52.
(89) Everest, A. M., Wallin, S. A., Stemp, E. D. A., Nocek, J. M., Mauk, A. G., and Hoffman, B. M. (1991) Aromatic hole superexchange through position-82 of cytochrome-c is not required for intracomplex electron-transfer to zinc cytochrome-c peroxidase. *J. Am. Chem. Soc. 113*, 4337−4338.
(90) DeFelippis, M. R., Murthy, C. P., Broitman, F., Weinraub, D., Faraggi, M., and Klapper, M. H. (1991) Electrochemical properties of tyrosine phenoxy and tryptophan indolyl radicals in peptides and amino acid analogs. *J. Phys. Chem. 95*, 3416−3419.
(91) Matelkova, K., Ossberger, K., Hudak, J., Vatral, J., Boca, R., and Linert, W. (2013) Redox activity of some non-innocent amino acids. *Monatsh. Chem. 144*, 937−949.
(92) Battistuzzi, G., Bellei, M., Bortolotti, C. A., and Sola, M. (2010) Redox properties of heme peroxidases. *Arch. Biochem. Biophys. 500*, 21−36.
(93) Purcell, W., and Erman, J. E. (1976) Cytochrome c peroxidase catalyzed oxidations of substitution inert iron (II) complexes. *J. Am. Chem. Soc. 98*, 7033−7037.
(94) Mondal, M. S., Fuller, H. A., and Armstrong, F. A. (1996) DIrect measurement of the reduction potential of catalytically active cytochrome c peroxidase compound. i: voltammetric detection of a reversible, coo perative two-electron transfer reaction. *J. Am. Chem. Soc. 118*, 263−264.
(95) Stevenson, G. P., Lee, C. Y., Kennedy, G. F., Parkin, A., Baker, R. E., Gillow, K., Armstrong, F. A., Gavaghan, D. J., and Bond, A. M. (2012) Theoretical analysis of the two-electron transfer reaction and experimental studies with surface-confined cytochrorne c peroxidase using large-amplitude fourier transformed AC voltammetry. *Langmuir 28*, 9864−9877.
(96) Barrows, T. P., Bhaskar, B., and Poulos, T. L. (2004) Electrostatic control of the tryptophan radical in cytochrome c peroxidase. *Biochemistry 43*, 8826−8834.
(97) Miller, M. A., Liu, R. Q., Hahm, S., Geren, L., Hibdon, S., Kraut, J., Durham, B., and Millett, F. (1994) Interaction domain for the reaction of cytochrome-c with the radical and the oxyferryl heme in cytochrome-c peroxidase compound-I. *Biochemistry 33*, 8686−8693.
(98) Lett, C. M., and Guillemette, J. G. (2002) Increasing the redox potential of isoform 1 of yeast cytochrome c through the modification of select haem interactions. *Biochem. J. 362*, 281.
(99) Rafferty, S. P., Pearce, L. L., Barker, P. D., Guillemette, J. G., Kay, C. R., Smith, M., and Mauk, A. G. (1990) Electrochemical, kinetic, and circular dicrhoic consequences of mutations at position 82 of yeast iso-1-cytochrome c. *Biochemistry 29*, 9365−9369.
(100) Machczynski, M. C., Kuhl, K. P., and McGuirl, M. A. (2007) Modulation of the electrochemical behavior of tyrosyl radicals by the electrode surface. *Anal. Biochem. 362*, 89−97.
(101) Hoganson, C. W., and Tommos, C. (2004) The function and characteristics of tyrosyl radical cofactors. *Biochim. Biophys. Acta, Bioenerg. 1655*, 116−122.
(102) Glover, S. D., Jorge, C., Liang, L., Valentine, K. G., Hammarstrom, L., and Tommos, C. (2014) Photochemical Tyrosine Oxidation in the Structurally Well-Defined alpha Y-3 Protein: Proton-Coupled Electron Transfer and a Long-Lived Tyrosine Radical. *J. Am. Chem. Soc. 136*, 14039−14051.
(103) Furuta, K., Tanizawa, Y., Horiuchi, H., Hiratsuka, H., and Okutsu, T. (2008) Tryptophan neutral radical brings along photochemical crystallization. *Chem. Lett. 37*, 458−459.
(104) Huyett, J. E., Doan, P. E., Gurbiel, R., Houseman, A. L. P., Sivaraja, M., Goodin, D. B., and Hoffman, B. M. (1995) Compound es of cytochrome-c peroxidase contains a trp pi-cation radical - characterization by cw and pulsed q-band endor spectroscopy. *J. Am. Chem. Soc. 117*, 9033−9041.
(105) Bonagura, C. A., Sundaramoorthy, M., Pappa, H. S., Patterson, W. R., and Poulos, T. L. (1996) An engineered cation site in cytochrome c peroxidase alters the reactivity of the redox active tryptophan. *Biochemistry 35*, 6107−6115.
(106) Bonagura, C. A., Bhaskar, B., Shimizu, H., Li, H. Y., Sundaramoorthy, M., McRee, D. E., Goodin, D. B., and Poulos, T. L. (2003) High-resolution crystal structures and spectroscopy of native and compound I cytochrome c peroxidase. *Biochemistry 42*, 5600−5608.
(107) Wang, J. M., Mauro, J. M., Edwards, S. L., Oatley, S. J., Fishel, L. A., Ashford, V. A., Nguyen, H. X., and Kraut, J. (1990) X-Ray structures of recombinant yeast cytochrome-c peroxidase and 3 heme-cleft mutants prepared by site-directed mutagenesis. *Biochemistry 29*, 7160−7173.
(108) Ferrer, J. C., Turano, P., Banci, L., Bertini, I., Morris, I. K., Smith, K. M., Smith, M., and Mauk, A. G. (1994) Active-site coordination chemistry of the cytochrome-c peroxidase asp235ala variant - spectroscopic and functional-characterization. *Biochemistry 33*, 7819−7829.
(109) Fishel, L. A., Farnum, M. F., Mauro, J. M., Miller, M. A., Kraut, J., Liu, Y. J., Tan, X. L., and Scholes, C. P. (1991) Compound-I radical in site-directed mutants of cytochrome-c peroxidase as probed by electron-paramagnetic resonance and electron nuclear double-resonance. *Biochemistry 30*, 1986−1996.
(110) Jonsson, M., Lind, J., Merenyi, G., and Eriksen, T. (1995) N-H bond dissociation energies, reduction potentials and pKa's of multisubstituted anilines and aniline radical cations. *J. Chem. Soc., Perkin Trans. 2 2*, 61−65.
(111) Wardman, P. (1989) Reduction potentials of one-electorn couples involving free radicals in aqueous solution. *J. Phys. Chem. Ref. Data 18*, 1637−1754.

DOI: 10.1021/acs.biochem.6b00262
Biochemistry 2016, 55, 4807−4822